Available online at www.sciencedirect.com

SCIENCE DIRECT®

Lithos 83 (2005) 347–370

LITHOS

www.elsevier.com/locate/lithos

Origin of micro-layering in a deep magma chamber: Evidence from two ultramafic–mafic layered xenoliths from Puy Beaunit (French Massif Central)

Olivier Féménias[a,*], Daniel Ohnenstetter[b], Nicolas Coussaert[c], Julien Berger[a], Daniel Demaiffe[a]

[a]*Laboratoire de Géochimie Isotopique et Géodynamique Chimique, DSTE, Université Libre de Bruxelles (CP 160/02) 50, av. Roosevelt 1050 Bruxelles, Belgique, Belgium*
[b]*CRPG-CNRS BP20 15, rue Notre Dame des Pauvres 54501 Vandoeuvre les Nancy Cedex, France*
[c]*Unité de Minéralogie et Géochimie, Musée Royal de l'Afrique Centrale, B-3080 Tervuren, Belgium*

Received 9 January 2004; accepted 18 February 2005
Available online 21 April 2005

Abstract

The origin of magmatic layering is still hotly debated. To try to shed some light on this problem, two ultramafic–mafic layered xenoliths from Puy Beaunit (French Massif Central) were investigated in detail. The nodules belong to a stratiform intrusion emplaced in the deep crust during the Permian (257 ± 6 Ma; Féménias, O., Coussaert, N., Bingen, B., Whitehouse, M., Mercier, J.-C., Demaiffe, D., 2003. A Permian underplating event in late- to post-orogenic tectonic setting. Evidence from the mafic–ultramafic layered xenoliths from Beaunit (French Massif Central). Chem. Geol. 199 293–315.). The 3 to 5 cm thick nodules have, in common, a central orthopyroxenite layer; the succession of layers is, respectively, norite–orthopyroxenite–norite (PBN 00-01) and norite–orthopyroxenite–harzburgite (PBN 00-03). The variations of both major (by electron microprobe) and trace, essentially the RE, elements (by LA-ICP-MS) were measured in major mineral phases (orthopyroxene, clinopyroxene, plagioclase, spinel) along cross-section perpendicular to the layering. Strong grain size, chemical and textural variations occur along these sections: they can be continuous or discontinuous, symmetrical or asymmetrical. Such complex variations cannot be solely related to a single magmatic history (fractional crystallisation, mineral sorting). Other processes such as element enrichment by residual liquid channelling along layer boundaries and/or sub-solidus recrystallisation and element redistribution must be invoked. It appears, in particular, that element distribution in the central orthopyroxenite layer could result from the injection of micro-sills of orthopyroxene-rich liquid between previously consolidated layers.

Keywords: Ultramafic–mafic xenolith; Layered intrusion; Sill; Deep magma chamber; Granulite facies

* Corresponding author. Tel.: +32 2 650 22 54; fax: +32 2 650 22 26.
E-mail address: ofemenia@ulb.ac.be (O. Féménias)

0024-4937/$ - see front matter © 2005 Elsevier B.V. All rights reserved.
doi:10.1016/j.lithos.2005.03.010

1. Introduction

Since the pioneering work of Wager and Deer (1939) on the Skaergaard layered intrusion, the mechanism of formation of igneous layering has been hotly debated. The cumulus model, originally proposed by Wager et al. (1960) and later expanded by Wager and Brown (1968) and Irvine (1982), has long been considered as "the paradigm". The layered rocks result from the interaction between melt and solid phases. Igneous layering occurs at all scales, from thick (several km) units, that are sometimes cyclic or rhythmic, to very thin (varying from inch layering to one crystal wide) micro-layers. The modal variations inside a unit are explained by fractional crystallisation/differentiation of the parental magma accompanied by crystal segregation. The succession of macro-units is related to repeated pulses of magma inside the chamber (replenishment events) and the succession of micro-units (layers or laminae) to chemical fronts. Recent studies have however shown that the "cumulate paradigm has to be reconsidered" (McBirney and Hunter, 1995) because it cannot explain all the petrographic features of the cumulate rocks, especially their texture development (Hunter, 1996). In their review of the modes of formation of igneous layering, Naslund and McBirney (1996) have identified 25 mechanisms operating during magma emplacement (4 mechanisms), in response to magma convection patterns (3 mechanisms), related to mechanical sorting (6 processes), due to variations in intensive parameters (6 processes) and occurring during late-stage crystallisation and cooling (6 processes).

Petrographic and geochemical investigations of layered intrusions (e.g. Cawthorn, 1996) have mainly been performed on rocks sampled through the whole stratigraphic column (several hundreds to thousands of metres in thickness). In contrast with this large scale layering, small-scale layering (that can be observed in hand specimens) has not been so intensively studied. Two recent studies have proposed unconventional mechanisms to explain the small-scale layering. Zingg (1996) has suggested that the stratification of the layered rocks of the Bushveld complex into orthopyroxene- and plagioclase-rich layers can be explained by the late sub-solidus recrystallisation of the cumulus minerals in a fluid gradient (variations of water activity linked to the emplacement of the Reef pegmatites). In another geological context, millimetre-scale modal layering observed in the upper solidification zone of sheets of magma and thick basalt flows (Philpotts and Dickson, 2002) has been related to rhythmic nucleation and growth of mineral clusters in a rapidly advancing thermal boundary layer.

We feel that the detailed study of finely layered rocks (micro-layering) can shed some light on the mechanism of formation of igneous layering. In this work, two layered ultramafic–mafic xenoliths from Puy Beaunit Quaternary volcano (French Massif Central) have been investigated in details. The two samples are both characterised by a central orthopyroxenite layer. Variations in both major and trace element composition of major mineral phases (orthopyroxene, olivine, plagioclase and spinel) in cross-sections perpendicular to the layering have been determined. It will be shown that the strong chemical and textural variations across the tow samples can tentatively be interpreted in terms of magmatic, metasomatic and sub-solidus events affecting the rocks. This study shows that the compositional variations of the main mineral phases cannot be explained by simple fractional crystallisation trends, related to a cumulation mechanism. It will stress the importance of post-cumulus processes such as late-emplacement inter-layers injection, fluid percolation and sub-solidus recrystallisation. In addition, it will be suggested that the orthopyroxene horizons were formed as microsill-like injections along pre-existing discontinuities in the layered sequence.

2. Geological setting

Puy Beaunit is a Quaternary maar (Baudry and Camus, 1970; Camus, 1975), dated at 43,900 ± 5100 Ma (Rosseel, 1996) and situated at the northernmost end of the Chaîne des Puys in the French Massif Central (Fig. 1). Its scoria cones contain abundant and varied mantle and crustal xenoliths so that it is one of the most diverse xenolith occurrences in the region (Brousse and Rudel, 1964; Mercier, 1972; Leyreloup, 1973; Berger, 1981; Downes and Dupuy, 1987; Lenoir et al., 2000; Féménias et al., 2001; Downes et al., 2003). Recently, Féménias et al. (2001) described two distinct populations of ultramafic xenoliths: (i) peridotites and pyroxenites derived from

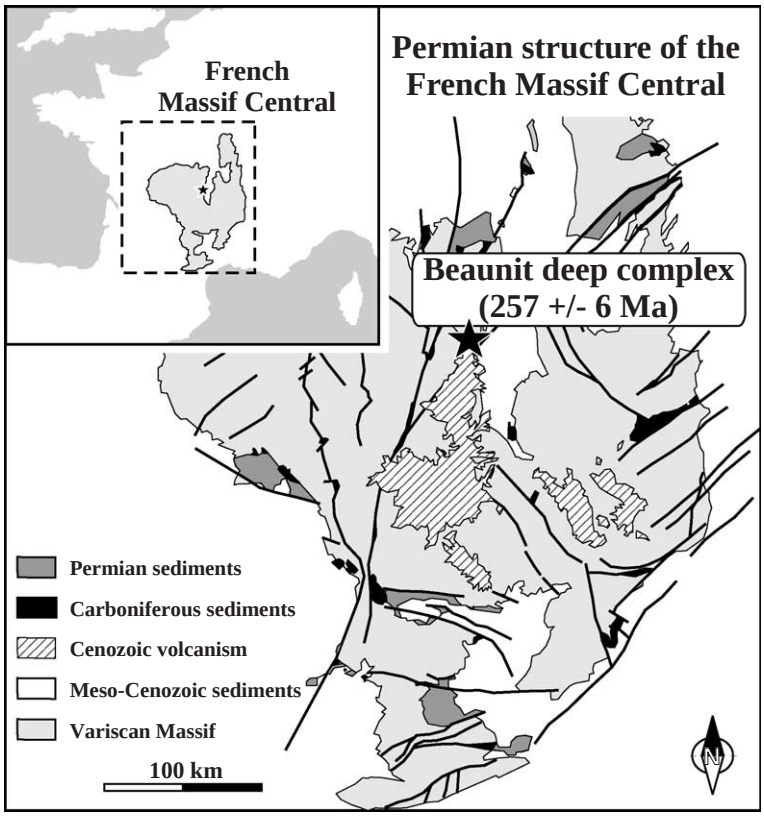

Fig. 1. Sketch maps showing location of Puy Beaunit and geological setting of Beaunit deep complex (modified after Féménias et al., 2003).

a differentiated plutonic complex and (ii) peridotites of mantle origin interpreted as residues of partial melting. The plutonic mafic to ultramafic xenoliths commonly show asymmetric layering on a millimetre to centimetre scale. The lithology of the layered xenoliths is highly variable: plagioclase-bearing mafic types (gabbro, gabbronorite, anorthositic gabbro), ultramafic types (peridotites, pyroxenite) and rare chromite-rich horizons have been described. The range of xenolith composition is comparable to the various lithologies observed in typical layered intrusions. Petrographic observations, mineral chemistry (orthopyroxene, plagioclase) and geochemical data obtained both on whole-rock unlayered samples and on minerals from layered nodules have shown that the magmatic peridotites, the pyroxenites and the gabbros could be derived from a single deep layered intrusion (Féménias et al., 2001, 2003). This intrusion was emplaced at the crust–mantle boundary (Faure et al., 2001; Féménias et al., 2001), during a Permian late- to post-orogenic under-plating event (SIMS U–Pb zircon age: 257 ± 6 Ma; Féménias et al., 2003).

The geochemistry of Puy Beaunit ultramafic–mafic xenoliths has been discussed by Féménias et al. (2003). The whole-rock trace element compositions are quite similar, particularly the REE patterns, to those of ultramafic cumulates in layered intrusions, e.g. the Lower and Lower Central Zones of the Bushveld complex (Maier and Barnes, 1998). The trace element and REE concentrations of igneous cumulates are largely governed by the proportion of interstitial trapped liquid (Barnes, 1986) and by their stratigraphic position. In randomly sampled xenoliths, the stratigraphic position of the samples is obviously unknown. Moreover, sub-solidus reequilibration textures tend to blur the primary magmatic textures (Leyreloup, 1973; Faure et al., 2001; Féménias et al., 2003). Nevertheless, the quite high incompatible trace element contents in the pyroxenites and lherzolites of Beaunit suggest a high proportion of post-cumulus

liquid; these rocks probably displayed meso- to orthocumulate textures originally. In contrast, dunites and harzburgites have significantly lower incompatible trace element contents; they presumably had an original adcumulate texture. The gabbroic xenoliths show strong whole-rock variations in incompatible element concentrations (unpublished data) that are very difficult to relate to each other. Nevertheless, some correlations have been observed between mineralogical composition and textures for some xenoliths, indicating a possible crystallisation sequence. Olivine and orthopyroxene were primary cumulus phases, followed by clinopyroxene and plagioclase. Rare intercumulus accessory phases like apatite, rutile and zircon occur in the most differentiated layers. The common negative Eu anomaly of some pyroxenites could be related to plagioclase fractionation; gabbroic and even gabbroic anorthosite layers have indeed been observed (Féménias et al., 2003). Homogeneous ultramafic xenoliths, interpreted as single cumulate layers up to 10 cm thick, have a calc-alkaline geochemical signature with LREE and LILE enrichments relative to Nb, Ta and Ti.

The xenolithic nature of the Beaunit layered rocks precludes a general structural and stratigraphic investigation of the differentiated complex. Nevertheless, the large size of some xenoliths (up to 10 cm) allows a detailed study of the layering of complex xenoliths to assess the influence and magnitude of magmatic and sub-solidus processes that occurred in the magma chamber at the crust–mantle boundary.

3. Analytical methods

The modal proportions (orthopyroxene, clinopyroxene, olivine, spinel and plagioclase) for each layer of the ultramafic–mafic xenoliths selected for this

Table 1
Selected representative microprobe analyses (major elements in wt.%, structural formulas) for orthopyroxenes

Sample	00-01	00-01	00-01	00-01	00-01	00-01	00-01	00-01	00-01	00-03	00-03	00-03	00-03	00-03
Layer	A	A	B	C	C	D	E	E	F	A	B	D	E	E
Type	opx rim	opx core	opx	opx	opx	opx	opx	opx	opx	opx core	opx core	opx core	opx core	opx core
SiO_2	50.75	48.95	49.17	51.84	53.17	53.34	53.19	52.02	49.89	51.63	52.48	51.85	53.48	52.50
TiO_2	0.06	0.24	0.26	0.16	0.09	0.15	0.11	0.16	0.24	0.30	0.17	0.23	0.04	0.13
Al_2O_3	7.32	9.09	9.42	5.08	4.12	3.97	4.19	4.86	7.37	3.39	3.82	4.88	2.93	3.60
FeO	14.32	15.08	14.25	13.09	12.73	11.93	12.37	12.95	14.18	13.29	13.08	13.69	16.75	14.76
MnO	0.15	0.13	0.20	0.37	0.19	0.26	0.23	0.11	0.26	0.35	0.35	0.23	0.29	0.25
MgO	27.10	25.63	26.42	28.23	29.19	29.13	28.95	28.71	27.20	29.66	29.21	28.38	25.62	27.95
CaO	0.30	0.13	0.23	0.29	0.33	0.24	0.30	0.37	0.15	0.90	0.26	0.58	0.53	0.38
Na_2O	0.04	0.01	0.00	0.00	0.03	0.00	0.00	0.00	0.02	0.06	0.00	0.00	0.00	0.06
K_2O	0.00	0.00	0.00	0.04	0.02	0.01	0.00	0.04	0.01	0.00	0.03	0.00	0.01	0.00
Cr_2O_3	0.09	0.11	0.18	0.33	0.31	0.19	0.11	0.11	0.00	0.10	0.16	0.08	0.00	0.00
Total	100.13	99.37	100.12	99.44	100.18	99.24	99.46	99.33	99.30	99.68	99.57	99.92	99.67	99.62
Si	1.818	1.774	1.763	1.863	1.889	1.905	1.898	1.867	1.804	1.861	1.883	1.859	1.942	1.895
Al^{IV}	0.157	0.205	0.211	0.118	0.093	0.091	0.094	0.110	0.165	0.083	0.089	0.112	0.064	0.081
Al^{VI}	0.152	0.184	0.187	0.097	0.079	0.075	0.083	0.096	0.149	0.061	0.073	0.094	0.061	0.073
Ti	0.001	0.007	0.007	0.004	0.002	0.004	0.003	0.004	0.006	0.008	0.005	0.006	0.001	0.003
Fe	0.429	0.457	0.427	0.394	0.378	0.356	0.369	0.389	0.429	0.401	0.392	0.410	0.509	0.445
Mn	0.005	0.004	0.006	0.011	0.006	0.008	0.007	0.003	0.008	0.011	0.011	0.007	0.009	0.008
Mg	1.447	1.385	1.412	1.512	1.546	1.551	1.540	1.536	1.466	1.594	1.562	1.517	1.387	1.504
Ca	0.011	0.005	0.009	0.011	0.012	0.009	0.012	0.014	0.006	0.035	0.010	0.022	0.021	0.015
Na	0.003	0.000	0.000	0.000	0.002	0.000	0.000	0.000	0.002	0.004	0.000	0.000	0.000	0.004
Cr	0.003	0.003	0.005	0.009	0.009	0.005	0.003	0.003	0.000	0.003	0.004	0.002	0.000	0.000
En	76.5	74.8	76.2	78.4	79.6	80.6	79.9	79.1	76.8	78.1	79.1	77.5	72.0	76.3
Fs	22.9	24.9	23.4	21.0	19.8	18.9	19.5	20.2	22.9	20.2	20.4	21.3	26.9	23.0
Wo	0.6	0.3	0.5	0.6	0.6	0.5	0.6	0.7	0.3	1.7	0.5	1.1	1.1	0.7
$Mg^{\#}$	77.1	75.2	76.8	79.4	80.3	81.3	80.7	79.8	77.4	79.9	79.9	78.7	73.2	77.1

$Fe = Fe^{2+} + Fe^{3+}$; $Mg^{\#} = Mg/(Mg+Fe)*100$.

study were determined by image analysis on polished thick (150 μm) sections. The separate layers of the two xenoliths have been classified according the IUGS classification (Streckeisen, 1974; Le Maitre, 2002). Representative electron microprobe data of the main mineral phases (plagioclase, olivine, pyroxenes and accessory minerals) are listed in Tables 1–6. Mineral analyses were performed on a Camebax SX 50 Microprobe at the University of Nancy (France). The operating conditions were an accelerating voltage of 15 kV, a beam current of 10 nA and a count time per element of 10 s for major elements and 20 s for minor elements. For accessory minerals, a bivoltage program was used with 15 kV for major elements and 20 kV for trace elements. Standards used were a combination of natural and synthetic minerals. Data correction used a PAP method correction (Pouchou and Pichoir, 1991).

Table 2
Selected representative microprobe analyses (major elements in wt.%, structural formulas) for clinopyroxenes

Sample	00-01	00-01	00-01	00-01	00-01	00-01
Layer	Lava	C	D	D	D	D
Type	cpx	cpx	cpx	cpx	cpx	cpx
SiO_2	47.33	49.90	50.49	49.96	50.21	52.31
TiO_2	2.63	1.31	0.82	1.32	1.20	0.19
Al_2O_3	5.03	6.00	4.22	5.11	4.88	1.48
FeO	10.20	3.71	6.53	3.49	5.76	4.85
MnO	0.18	0.09	0.08	0.11	0.05	0.12
MgO	13.35	14.46	16.31	15.22	15.69	17.70
CaO	20.31	23.78	21.03	23.95	21.38	22.74
Na_2O	0.40	0.32	0.08	0.20	0.29	0.07
K_2O	0.06	0.02	0.06	0.02	0.02	0.00
Cr_2O_3	0.00	0.40	0.32	0.30	0.22	0.03
Total	99.48	99.97	99.98	99.72	99.90	99.63
Si	1.794	1.833	1.864	1.840	1.853	1.931
Al^{IV}	0.207	0.180	0.125	0.162	0.150	0.039
Al^{VI}	0.018	0.080	0.058	0.061	0.062	0.026
Ti	0.075	0.036	0.023	0.037	0.033	0.005
Fe	0.323	0.114	0.202	0.107	0.178	0.150
Mn	0.006	0.003	0.003	0.003	0.002	0.004
Mg	0.754	0.792	0.897	0.836	0.863	0.974
Ca	0.825	0.936	0.832	0.945	0.846	0.899
Na	0.029	0.023	0.006	0.015	0.020	0.005
Cr	0.000	0.011	0.009	0.009	0.007	0.001
En	39.5	42.9	46.4	44.2	45.7	48.1
Fs	17.3	6.3	10.6	5.9	9.5	7.6
Wo	43.2	50.7	43.0	50.0	44.8	44.4
$Mg^{\#}$	70.0	87.4	81.7	88.6	82.9	86.7

$Fe = Fe^{2+} + Fe^{3+}$.

Table 3
Selected representative microprobe analyses (major elements in wt.%, structural formulas) for olivines

Sample	00-03	00-03	00-03	00-03
Layer	A	A	A	C
Type	ol	ol	ol	ol
SiO_2	39.13	38.62	38.80	37.25
TiO_2	0.00	0.03	0.03	0.21
Al_2O_3	0.00	0.02	0.03	0.00
FeO	19.16	19.32	19.37	20.90
MnO	0.30	0.29	0.27	0.15
MgO	41.10	40.88	41.08	41.07
CaO	0.11	0.13	0.11	0.12
NiO	0.22	0.31	0.34	0.11
Total	100.02	99.59	100.01	99.82
Si	1.003	0.998	0.998	0.968
Al	0.000	0.001	0.001	0.000
Ti	0.000	0.001	0.001	0.004
Fe	0.411	0.417	0.417	0.454
Mn	0.006	0.006	0.006	0.003
Mg	1.571	1.574	1.575	1.591
Ca	0.003	0.003	0.003	0.003
Ni	0.007	0.005	0.004	0.002
$Mg^{\#}$	79.3	79.0	79.1	77.8

Trace elements in orthopyroxene and plagioclase were analysed by in situ Laser Ablation ICP-MS (Tables 7 and 8). The data were collected with a UV Fison laser probe coupled to a VG elemental Plasmaquad (PQ2 Turbo Plus) ICP-MS (Musée Royal de l'Afrique Centrale at Tervuren). The laser ablation microprobe is based on a Continuum Minilite Q-switched Nd: YAG laser operating in the far-UV (266 nm) wavelengths. The power of output beam is maximum (2 mJ/pulse) for a 10 Hz repetition rate of pulse, that is attenuated to obtain the required energy to get the appropriate crater size. The typical size of the crater is in the range 40 to 60 μm. The focusing on the sample is done manually through a high magnification lens (1500×). Each sample and standard was ablated for 27 s, corresponding to 12 s of pre-ablation to clean the surface and stabilise the ablation, followed by 15 s of data acquisition. The raw data on each isotope peak were subtracted from the gas blanks and normalised to the ^{43}Ca signal and then compared to calibration lines. The calibration lines are based on the spiked NIST 612 synthetic standard and two laboratory mineral standards: a pyrope megacryst from the Shavaryn–Tsaram basalts (Mongolia) and a Cr-diopside from

Table 4
Selected representative microprobe analyses (major elements in wt.%, structural formulas) for plagioclases

Sample	00-01	00-01	00-01	00-01	00-01	00-01	00-03	00-03	00-03
Layer	A	A	B	E	F	Lava	E	E	E
Type	pl rim	pl core	pl crack	pl int	pl core	pl core	pl core	pl core	pl core
SiO_2	46.66	52.24	54.72	43.07	44.45	50.88	51.71	49.34	46.15
TiO_2	0.07	0.00	0.04	0.00	0.03	0.17	0.03	0.05	0.00
Al_2O_3	32.86	29.48	27.90	35.68	34.75	30.05	29.84	31.07	33.57
FeO	0.36	0.22	0.63	0.60	0.54	0.94	0.31	0.36	0.28
MnO	0.09	0.00	0.03	0.00	0.05	0.00	0.00	0.00	0.04
MgO	0.07	0.09	0.11	0.12	0.08	0.11	0.06	0.06	0.07
CaO	16.11	12.65	10.30	19.85	18.88	13.97	13.52	15.19	17.86
Na_2O	2.39	4.50	5.60	0.40	0.79	3.63	3.53	2.65	1.33
K_2O	0.17	0.40	0.56	0.00	0.00	0.37	0.52	0.37	0.12
Total	98.77	99.59	99.90	99.72	99.58	100.11	99.23	98.75	99.14
Si	2.174	2.387	2.482	2.008	2.068	2.328	3.871	3.863	3.871
Al	1.805	1.588	1.491	1.961	1.905	1.621	0.046	0.048	0.051
Ca	0.804	0.619	0.501	0.992	0.941	0.685	0.019	0.021	0.025
Na	0.216	0.399	0.493	0.036	0.071	0.322	0.009	0.007	0.003
K	0.010	0.024	0.032	0.000	0.000	0.022	0.001	0.001	0.000
Or	1.0	2.3	3.2	0.0	0.0	2.1	3.0	2.2	0.7
Ab	21.0	38.3	48.0	3.5	7.0	31.3	31.1	23.5	11.8
An	78.1	59.4	48.8	96.5	93.0	66.6	65.9	74.3	87.5

the Inagly Dunite Massif (Siberia). Typical detection limits, precision and accuracy of the methods are detailed in Féménias et al. (2003).

4. Sample description, petrography and mineral composition

The two layered samples that have been selected for detailed in situ chemical investigation are: PBN 00-01 (Fig. 2a) which contains the zircon investigated by SIMS (Féménias et al., 2003) and PBN 00-03 (Fig. 2b). These centimetre-scale xenoliths (respectively 3 and 5 cm) are composite mafic–ultramafic layered rocks that represent one of the most common petrographic types in the Beaunit xenolith population. The rocks are fresh, completely devoid of lava veinlets. Pyrometamorphic effect is restricted to a very thin (<1 mm) zone at the contact between the xenolith and the host lava. Orthopyroxene and plagioclase crystals of the xenolith are indeed zoned to slightly lower $Mg^{\#}$ and An content, respectively (i.e. Fig. 3a,c). The composite layered structure of the xenoliths induces a poor cohesion that sometimes results to the complete desegregation to loose grains when sampling. In thin-sections, the samples are medium- to fine-grained; they show numerous cracks that presumably develop during sampling and/or thin-section preparation. Both samples have a centimetre-scale symmetrical orthopyroxenite central layer, between two norite layers in PBN 00-01 and between norite and harzburgite layers in PBN 00-03 (Fig. 2).

4.1. Petrography

Sample PBN 00-01 (Fig. 2a) is composed of a norite–orthopyroxenite–norite sequence. The first norite layer (zone A on Fig. 2a) has approximately equal proportions of plagioclase and orthopyroxene with accessory (<6%) spinel. This 2 mm thick layer is at the contact between the host lava and the orthopyroxenite central layer. It is medium-grained (0.4–0.7 mm for the silicate phases; the spinel is smaller, down to 0.1 mm) with a polygonal texture and randomly distributed interstitial accessory phases. Shape orientation has not been observed. At the contact with the host lava, the norite has been mechanically and mineralogically affected. The contact of this norite with the adjacent orthopyroxenite central layer is very sharp. The central part of the sample is composed of a polygonal orthopyroxenite s.s. (>90% modal orthopyroxene). This 2 cm thick zone has been subdivided in 5 sub-

Table 5
Selected representative microprobe analyses (major elements in wt.%, structural formulas) for spinels

Sample	00-01	00-01	00-01	00-01	00-01	00-01	00-01	00-03	00-03	00-03	00-03	00-03	00-03
Layer	A	B	C	D	D	E	E	A	A	B	B	D	D
Type	spinel	spinel	spinel	spinel	spinel	spinel	spinel	spinel	spinel	spinel	spinel	spinel	spinel
SiO_2	0.00	0.07	0.07	0.08	0.05	0.06	0.04	0.06	0.07	0.00	0.08	0.00	0.07
TiO_2	1.03	1.05	0.37	0.35	0.40	0.60	0.27	0.60	1.30	0.63	0.46	0.49	0.45
Al_2O_3	53.46	47.71	51.31	52.48	51.94	48.03	61.32	45.45	43.88	51.66	55.23	54.88	56.39
FeO	28.76	21.39	20.65	20.47	19.70	19.70	16.37	30.61	31.97	23.61	20.58	22.74	21.06
MnO	0.19	0.07	0.16	0.16	0.19	0.11	0.19	0.09	0.31	0.05	0.17	0.02	0.16
MgO	15.30	14.65	15.62	15.40	15.64	14.43	18.10	14.18	13.67	15.39	16.46	15.87	16.80
CaO	0.03	0.00	0.03	0.00	0.00	0.02	0.00	0.00	0.00	0.00	0.00	0.04	0.01
Na_2O	0.00	0.04	0.00	0.00	0.00	0.00	0.00	0.00	0.00	0.02	0.00	0.00	0.03
K_2O	0.03	0.00	0.00	0.00	0.00	0.00	0.07	0.00	0.04	0.00	0.00	0.03	0.01
Cr_2O_3	0.39	13.37	10.46	9.86	11.06	15.06	2.50	7.49	6.90	6.60	5.40	4.06	4.10
NiO	0.04	0.45	0.34	0.38	0.20	0.34	0.40	0.36	0.29	0.25	0.27	0.27	0.12
Total	99.23	98.80	99.01	99.17	99.18	98.34	99.26	98.84	98.43	98.21	98.64	98.39	99.21
Si	0.000	0.016	0.016	0.016	0.011	0.013	0.008	0.013	0.017	0.000	0.016	0.000	0.016
Al	13.598	12.509	13.185	13.433	13.306	12.651	14.987	12.003	11.723	13.345	13.964	13.955	14.105
Ti	0.168	0.176	0.061	0.057	0.065	0.101	0.042	0.100	0.222	0.105	0.074	0.080	0.072
Fe^{2+}	3.184	3.209	2.906	2.990	2.939	3.220	2.317	3.291	3.483	3.025	2.751	2.903	2.694
Fe^{3+}	2.006	0.771	0.859	0.728	0.641	0.461	0.522	2.445	2.576	1.303	0.940	1.200	1.044
Mn	0.034	0.014	0.029	0.029	0.035	0.020	0.033	0.017	0.060	0.010	0.031	0.004	0.029
Mg	4.922	4.858	5.077	4.986	5.067	4.808	5.595	4.737	4.617	5.027	5.262	5.105	5.315
Cr	0.067	2.351	1.802	1.693	1.900	2.662	0.409	1.327	1.236	1.143	0.916	0.692	0.689
Ni	0.006	0.080	0.059	0.067	0.034	0.061	0.067	0.066	0.052	0.043	0.046	0.047	0.020
Ulvöspinel	2.1	2.2	0.8	0.7	0.8	1.3	0.5	1.3	2.8	1.3	0.9	1.0	0.9
Magnesiochromite	0.0	14.7	11.3	10.6	11.9	16.6	2.6	8.3	7.7	7.1	5.7	4.3	4.3
Spinel	61.6	46.1	52.2	51.7	51.4	43.5	67.4	50.9	50.1	55.8	60.1	59.5	62.2
Hercynite	23.0	31.9	29.8	31.9	31.4	35.3	25.9	23.9	22.5	27.5	26.8	27.8	25.6
Magnetite	12.0	3.7	4.6	3.7	3.5	2.0	2.3	14.3	15.3	7.6	5.3	6.7	6.1
$Mg^{\#}$	60.7	60.2	63.6	62.5	63.3	59.9	70.7	59.0	57.0	62.4	65.7	63.7	66.4

layers on the basis of grain-size variations. The whole layer is roughly symmetrical with a fine-grained (0.1 to 0.3 mm) inner band (zone D on Fig. 2a), characterised by the presence of accessory clinopyroxene and phlogopite (modal proportion <1vol.%). This inner layer passes progressively to medium-grained (0.2 to 0.7 mm) orthopyroxenite (zones C and E) and finally to coarse-grained (0.5 to 1.2 mm) outer orthopyroxenite (zones B and F). However, these orthopyroxenite sub-layers have slightly variable thickness (zone B is thicker than zone F) and mineral proportions (the spinel modal abundance is higher in zones E and D than in zones C and B). The last norite layer G contains about 65% orthopyroxene, 32% plagioclase and opaque minerals; it is fine-grained (0.2–0.4 mm) with a polygonal texture.

Sample PBN 00-03 (Fig. 2b) is composed of a norite–orthopyroxenite–harzburgite sequence. The norite layer (zones E1 and E2 on Fig. 2b) is essentially composed of plagioclase (51%) and orthopyroxene (43%) with accessory (~6%) Mg-ilmenite; the proportion of orthopyroxene slightly increases near the orthopyroxenite layer. The grain size is in the range 0.4–0.7 mm for the silicate phases, the opaque phases are smaller (down to 0.1 mm). The rock is a typical homogeneous medium-grained norite; there is no shape orientation. The texture is polygonal, the interstitial oxides are locally agglomerated. The central portion of the sample (zones B, C and D on Fig. 2b) is mainly a medium-grained orthopyroxenite (up to 90% orthopyroxene) with a thin (one crystal wide) layer of norite (zone C). The orthopyroxenite layer has a polygonal texture; it contains spinel instead of ilmenite. The last layer (zone A on Fig. 2b) is a harzburgite (84% olivine, 10–13% orthopyroxene and 2–7% opaques). Olivine and orthopyrox-

Table 6
Selected representative microprobe analyses (major elements in wt.%, structural formulas) for magnesio-ilmenites and armacolite

Sample	00-01	00-01	00-01	00-01	00-01	00-01	00-01	00-03	00-03	00-03	00-03	00-03	00-03	00-03	00-03
Layer	A	A	C	C	D	D	E	A	A	B	D	D	E	E	E
Type	Mg-il	Mg-il	Mg-il	Mg-il	Mg-il	Mg-il	Mg-il	Mg-il	Mg-il	Mg-il	Mg-il	Mg-il	Mg-il	Mg-il	Arm
SiO_2	0.07	0.00	0.05	0.11	0.10	0.03	0.00	0.00	0.00	0.00	0.00	0.00	0.01	0.02	0.00
TiO_2	53.98	54.20	54.94	54.47	56.06	57.03	55.43	55.67	56.28	55.34	57.42	54.84	54.90	55.47	70.33
Al_2O_3	0.75	0.64	0.47	0.57	0.32	0.40	0.68	0.33	0.66	0.31	0.58	0.47	0.57	0.30	0.57
FeO	35.92	32.30	30.57	30.34	31.00	28.71	30.49	32.54	30.31	31.41	30.16	33.91	33.52	35.69	20.84
MnO	0.49	0.18	0.29	0.23	0.24	0.31	0.44	0.20	0.32	0.46	0.32	0.23	0.17	0.41	0.05
MgO	8.61	10.35	11.58	11.21	10.83	12.38	11.63	9.19	10.96	10.15	11.28	9.66	9.48	8.36	7.98
CaO	0.07	0.09	0.02	0.06	0.01	0.05	0.00	0.02	0.05	0.00	0.05	0.11	0.00	0.01	0.02
Na_2O	0.00	0.00	0.00	0.00	0.06	0.00	0.10	0.00	0.03	0.00	0.00	0.06	0.00	0.00	0.03
K_2O	0.04	0.02	0.01	0.00	0.00	0.00	0.00	0.00	0.00	0.02	0.00	0.06	0.02	0.00	0.00
Cr_2O_3	0.24	1.20	1.34	1.69	0.64	0.21	0.07	1.07	0.52	0.91	0.46	0.68	0.27	0.15	0.14
NiO	0.08	0.10	0.16	0.27	0.11	0.04	0.11	0.13	0.05	0.00	0.00	0.00	0.02	0.07	0.08
Total	100.25	99.09	99.42	98.95	99.37	99.14	98.97	99.15	99.17	98.60	100.28	100.01	98.95	100.48	100.05
Al	0.047	0.040	0.029	0.035	0.020	0.024	0.042	0.021	0.041	0.020	0.036	0.029	0.036	0.019	0.037
Ti	2.144	2.152	2.157	2.153	2.216	2.235	2.180	2.235	2.225	2.216	2.244	2.168	2.198	2.211	2.861
Fe^{2+}	1.586	1.425	1.334	1.333	1.362	1.251	1.333	1.452	1.332	1.399	1.311	1.491	1.492	1.581	0.943
Mn	0.022	0.008	0.013	0.010	0.011	0.014	0.020	0.009	0.014	0.021	0.014	0.010	0.008	0.019	0.002
Mg	0.677	0.814	0.901	0.878	0.848	0.961	0.906	0.731	0.858	0.805	0.873	0.757	0.752	0.660	0.643
Cr	0.010	0.050	0.055	0.070	0.027	0.008	0.003	0.045	0.022	0.038	0.019	0.028	0.011	0.006	0.006
Ni	0.003	0.004	0.007	0.011	0.005	0.002	0.005	0.005	0.002	0.000	0.000	0.000	0.001	0.003	0.004
Geikielite	30.6	37.0	40.9	40.1	38.2	43.2	40.9	33.3	38.9	36.3	39.7	34.1	33.8	29.5	
Pyrophanite	1.0	0.4	0.6	0.5	0.5	0.6	0.9	0.4	0.6	0.9	0.6	0.5	0.3	0.8	
Ilmenite	65.4	60.6	56.4	57.8	61.2	56.2	56.3	66.2	60.4	62.6	59.6	63.6	64.6	68.5	
Hematite	3.0	2.1	2.1	1.6	0.1	0.0	1.9	0.0	0.0	0.2	0.0	1.8	1.2	1.1	
$Mg^{\#}$	29.9	36.4	40.3	39.7	38.4	43.5	40.5	33.5	39.2	36.5	40.0	33.7	33.5	29.4	40.6

Table 7
Selected representative trace elements analyses (ppm) in orthopyroxenes and plagioclases from sample PBN 00-01 determined by LA-ICP-MS

Sample	00-01	00-01	00-01	00-01	00-01	00-01	00-01	00-01	00-01	00-01
Layer	A	B	C	C	D	D	E	F	F	F
Type	opx 1	opx 1	opx2	opx 3	opx 2	opx 1	opx 1	opx 2	opx 1	pl
Spot	($n=7$)	($n=4$)	($n=5$)	($n=4$)	($n=5$)	($n=5$)	($n=5$)	($n=3$)	($n=3$)	($n=5$)
Ti	1133	713	959	905	440	391	350	320	376	148
Cr	1135	1512	1392	1282	466	609	148	59	94	14
Co	26	27	30	26	21	21	16	12	17	1
Ni	30	96	144	96	88	83	30	–	–	72
Sr	4.37	2.10	1.60	2.16	2.80	2.80	1.60	2.09	2.90	14.93
Zr	0.14	0.11	0.19	0.21	0.14	0.12	0.24	4.17	0.19	675
Nb	6.75	3.00	9.49	3.64	3.73	3.30	2.85	4.44	2.84	1.03
Y	0.40	0.36	0.55	0.51	0.35	0.25	0.30	0.29	0.39	0.26
La	0.03	0.08	0.03	0.09	0.06	0.01	0.03	0.05	0.06	16.14
Ce	0.12	0.30	0.14	0.33	0.21	0.17	0.13	0.28	0.17	31.82
Nd	0.31	0.49	0.16	0.34	0.13	0.29	0.13	0.27	0.16	18.47
Sm	0.15	0.24	0.11	0.04	0.06	0.09	0.07	0.10	0.07	2.17
Eu	0.02	0.03	0.05	0.04	0.03	0.01	0.01	0.06	<0.01	2.83
Gd	0.52	0.59	0.23	0.32	0.24	0.21	0.18	0.40	0.19	2.28
Dy	1.10	1.11	0.69	0.76	0.44	0.47	0.43	0.62	0.39	1.25
Er	0.80	1.06	0.60	0.69	0.66	0.48	0.38	0.54	0.37	0.42
Yb	0.83	0.79	0.72	0.83	0.51	0.50	0.56	0.48	0.30	0.27

Table 8
Selected representative rare earth elements analyses (ppm) in orthopyroxenes and plagioclases from sample PBN 00-03 determined by LA-ICP-MS

Sample	00-03	00-03	00-03	00-03	00-03	00-03	00-03	00-03	00-03	00-03	00-03	00-03
Layer	A	B	C	C	D	D	E	E	E(2)	E(2)	E(2)	E(2)
Type	opx 1	opx 1	opx 1	pl	opx 1	opx 2	opx 1	pl	opx 1	opx 2	opx 3	pl
Spot	($n=3$)	($n=6$)	($n=5$)	($n=5$)	($n=5$)	($n=4$)	($n=4$)	($n=6$)	($n=7$)	($n=5$)	($n=5$)	($n=6$)
La	0.02	0.02	0.03	3.45	0.02	0.07	0.03	5.10	0.03	0.02	0.37	5.30
Ce	0.07	0.06	0.06	6.12	0.08	0.20	0.12	7.95	0.07	0.07	0.77	9.10
Pr	0.01	0.01	0.02	0.59	0.01	0.03	0.02	0.92	0.02	0.02	0.07	0.95
Nd	0.06	0.08	0.09	2.47	0.09	0.16	0.09	4.01	0.13	0.09	0.30	4.07
Sm	0.04	0.05	0.06	0.48	0.02	0.07	0.04	0.79	0.08	0.05	0.05	0.77
Eu	0.01	0.01	0.02	1.59	<0.01	0.02	<0.01	1.45	0.02	0.02	0.01	2.48
Gd	0.14	0.21	0.16	0.49	0.18	0.17	0.15	1.16	0.36	0.27	0.22	1.01
Dy	0.22	0.41	0.40	0.31	0.55	0.32	0.61	0.92	0.81	0.73	0.62	0.73
Er	0.20	0.34	0.34	0.20	0.41	0.28	0.62	0.40	0.68	0.70	0.61	0.31
Yb	0.24	0.39	0.35	0.14	0.48	0.40	0.65	0.38	0.74	0.84	0.73	0.22
Lu	0.04	0.07	0.06	0.02	–	0.07	–	0.05	0.13	0.11	–	0.04

ene have slightly smaller grain sizes than in the orthopyroxenite or norite layers. Spinel is interstitial and randomly distributed. In contrast to the norite layer, the harzburgite shows significant shape orientation, parallel to the layering. The norite–orthopyroxenite boundary is characterised by a 6 mm-thick transition zone, whereas the orthopyroxenite–harzburgite boundary is sharp. The whole xenolith is crosscut by cracks, roughly orthogonal to the layering, some of them appear to be related to the host lava surrounding the nodule (Fig. 2b).

4.2. Mineral chemistry

4.2.1. Major silicate phases

The $Mg^{\#}$ (=Mg/(Mg+Fe)×100) of orthopyroxene from sample PBN 00-01 varies from 75 to 82% (Table 1 and Fig. 3a), defining a smooth and continuous trend from the norite layers (75–77) to the orthopyroxenite layer (77–82). There are no systematic differences between cores and rims of grains, except for pyroxenes from zone A that have rims with slightly lower $Mg^{\#}$ (75) than their cores ($Mg^{\#}=77$). This range of values is similar to the range (72–81) for orthopyroxene from PBN 00-03 (Table 1 and Fig. 3e) and also to the compositional range of orthopyroxenes from monolithologic mafic xenoliths and orthopyroxenites (Féménias et al., 2003). The orthopyroxenes of PBN 00-03 are unzoned and there is no significant compositional difference between the small and the large grains. The $Mg^{\#}$ varies continuously from 79–81 in the harzburgite layer to 77–80 in the orthopyroxenite layer and to 72–77 in the norite layer. In the central orthopyroxenite layer (zones B to F) of PBN 00-01, orthopyroxene composition varies symmetrically, with lower $Mg^{\#}$ (76–77%) near the upper and lower boundaries of the zone and slightly higher values ($Mg^{\#}=81$) in the fine-grained central zone D. In PBN 00-03, the $Mg^{\#}$ of orthopyroxene varies regularly from the norite ($Mg^{\#}\sim72$) to the orthopyroxenite zones ($Mg^{\#}\sim80$), that are thus asymmetrical, while it is roughly constant in the harzburgite zone.

Clinopyroxene occurs as interstitial grains (<50 μm) in the central orthopyroxenite zone of PBN 00-01 (Table 2 and Fig. 3b); it is absent in PBN 00-03. It displays a range of compositions ($80.5<Mg^{\#}<88.5$), comparable to clinopyroxenes of the websterite xenoliths (Féménias et al., 2003) and significantly different from augites in the host lava ($Mg^{\#}\sim70$).

Olivine is present in the harzburgite layer (Table 3 and Fig. 3f) of PBN 00-03. It has a uniform composition ($Mg^{\#}\sim79$); rare small interstitial olivines from zone C are slightly less magnesian (~77.7%) and more titaniferous (~0.0042 a.p.f.u.). The $Mg^{\#}_{opx}/Mg^{\#}_{ol}$ ratio is close to one, as observed in other Beaunit ultramafic cumulate xenoliths (Féménias et al., 2003). By contrast, mantle-derived harzburgite xenoliths from Beaunit have olivine and orthopyroxene with higher $Mg^{\#}$ (>88 for olivine and >88.5 for orthopyroxene; Féménias et al., 2003).

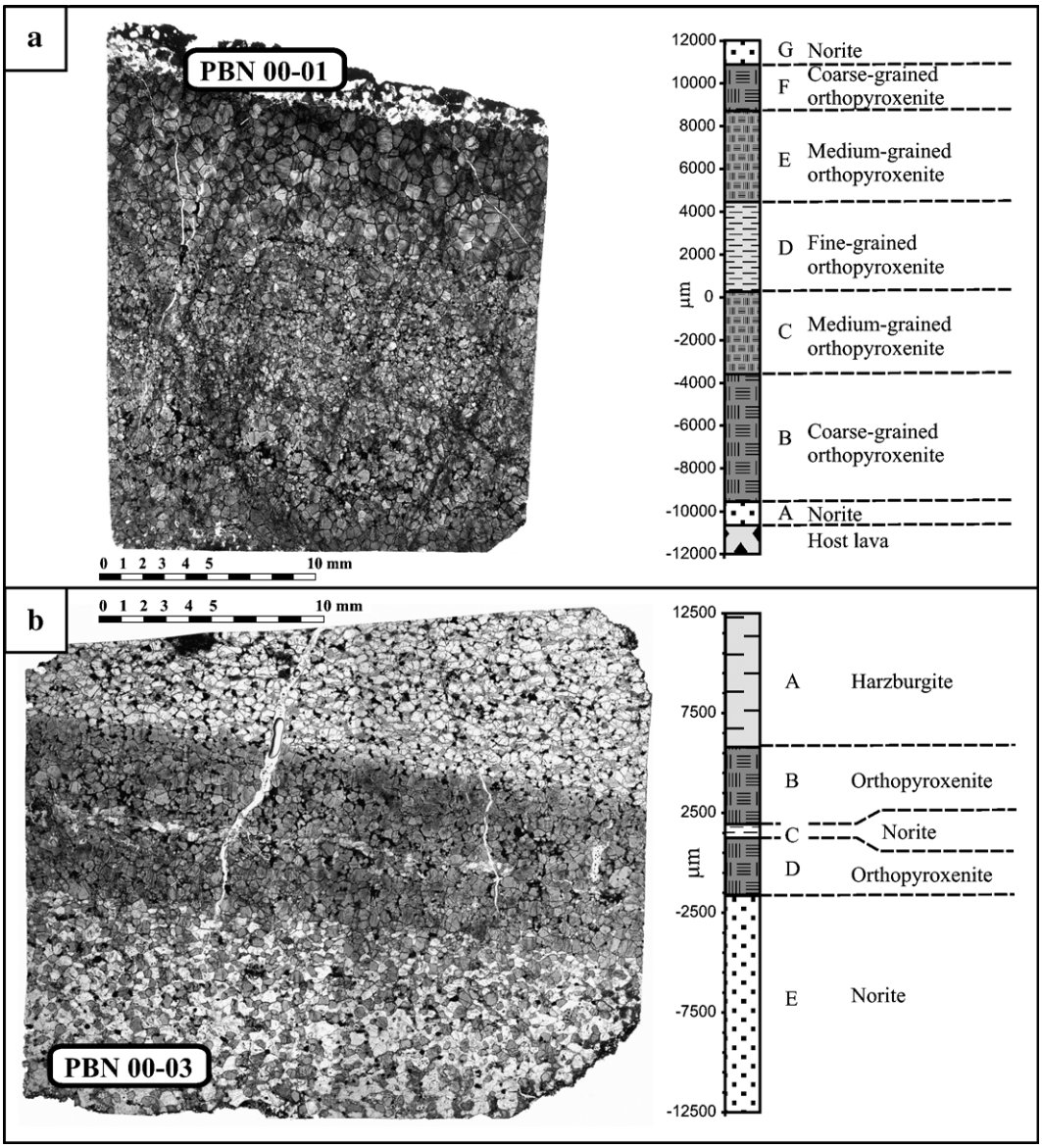

Fig. 2. Thick section photography and detailed lithological profile of samples PBN 00-01 (a) and PBN 00-03 (b).

The modal proportion of plagioclase in PBN 00-01 is low (Table 4 and Fig. 3c). Plagioclases from the norite (zone A) show strong reverse zoning, with a lower An content in the core (An_{60}) than in the rims (An_{80}). The rare interstitial plagioclases in the coarse- and medium-grained orthopyroxenites are homogeneous. They show a roughly symmetrical compositional trend with lower An values near the norites ($An_{88–91}$) than in the central zone D ($An_{96–98}$). Small plagioclases (<50 µm) in the cracks of zone B have a low An content (An_{42} to An_{59}), roughly comparable to those of the basalt ($An_{56.5–66.5}$); they probably crystallised during magma infiltration in the crack. In PBN 00-03, the plagioclase of norite layer E displays a large compositional range (An_{61}–An_{90}) (Table 4 and Fig. 3g). Plagioclase composition is

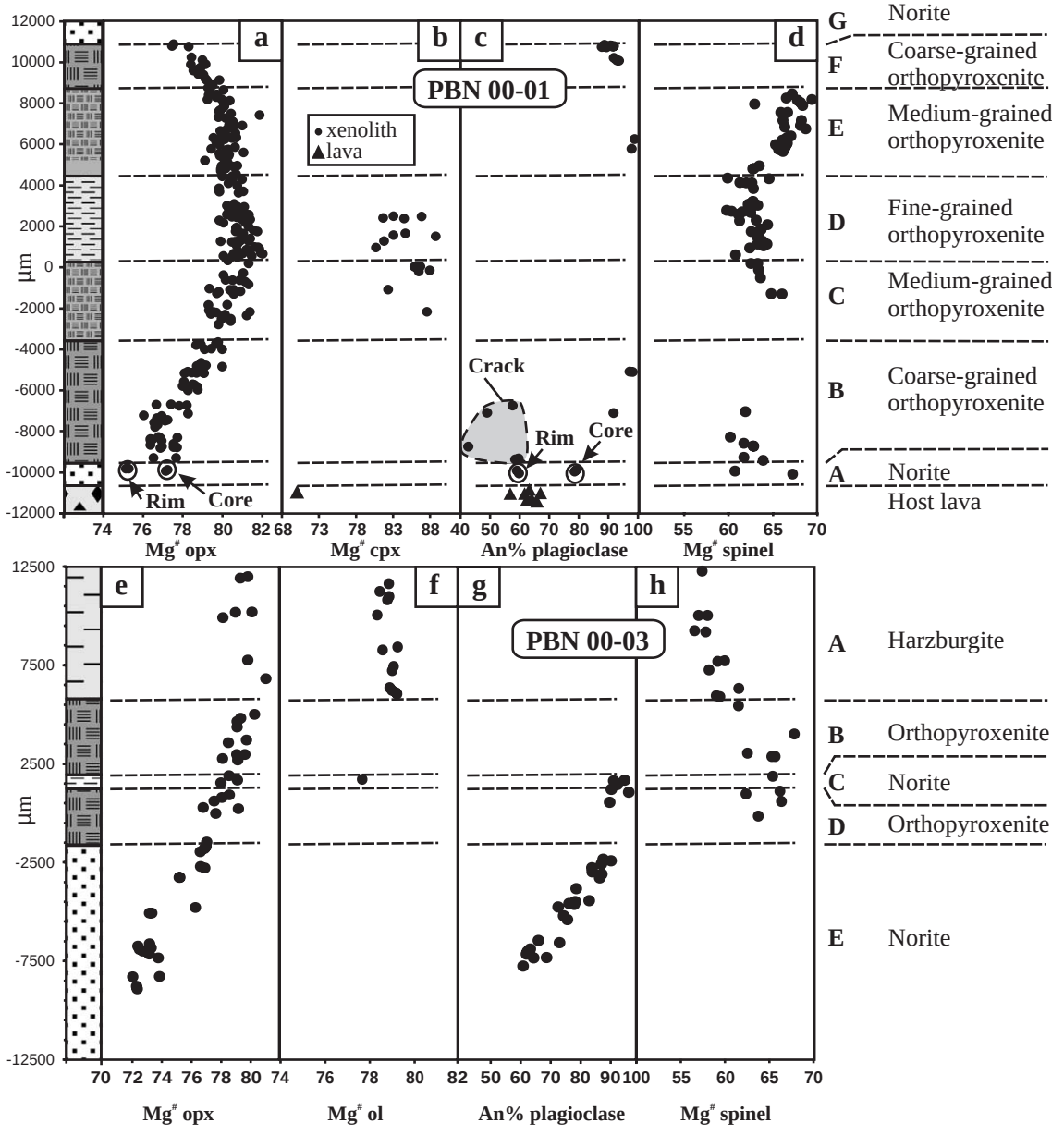

Fig. 3. Compositional variations of phases versus lithological profile. PBN 00-01: (a) orthopyroxene, (b) clinopyroxene, (c) plagioclase and (d) spinel. PBN 00-03: (e) orthopyroxene, (f) olivine, (g) plagioclase and (h) spinel. Dashed lines indicate lithological boundaries.

positively correlated with the $Mg^{\#}$ of orthopyroxene, the plagioclase close to the contact with the orthopyroxenite layer has the highest An content ($An_{85–90}$). Plagioclase from the thin central norite layer C has an An content (An_{92}) comparable to those of the orthopyroxenite layer.

4.2.2. Accessory phases

The $Mg^{\#}$ of core spinels from PBN 00-01 (Table 5 and Fig. 3d) is quite constant ($Mg^{\#}$ = 60–65) in zones A to D but increases up to 70 in zone E. In the latter, spinels have roughly higher Al, Mg and lower Fe (Fe^{2+} and Fe^{3+}), Cr and Ti contents, as well as lower

Fe^{3+}/Fe^{2+} ratios. Spinels from the orthopyroxenite central layer (Fig. 4b) display three distinct compositional domains, without any simple correlation inside each domain. In the central fine-grained zone D, they have a high $Cr^{\#}$ and a medium $Mg^{\#}$ (respectively 0.10–0.16 and 0.60–0.65 on Fig. 4b). In contrast, spinels from zones B and C show much lower $Cr^{\#}$ for comparable $Mg^{\#}$ values (respectively 0–0.02 and 0.61–0.63 on Fig. 4b). In zone E, spinel has intermediate $Cr^{\#}$ values and higher $Mg^{\#}$ values (respectively 0.02–0.10 and 0.61–0.71 on Fig. 4b). In this zone, spinel composition is roughly correlated with the position of the crystal in the layer.

In PBN 00-03, spinel is an accessory phase in zones A to D (Fig. 3h). It shows contrasting behaviour: its Cr/(Cr+Al) ratio is high (~0.10) in the harzburgite zone A (Fig. 4b) and lower (0.1–0.03) in the orthopyroxenite layer (zones B to D). Spinel compositions are not correlated with stratigraphic position in the layer. There is a broad compositional band suggesting a double substitution, $Al \Leftrightarrow Cr$ and $Mg \Leftrightarrow Fe^{2+}$. There is also a strong change in Fe^{3+}/Fe^{2+} ratios, from the harzburgite zone A (Fe^{3+}/Fe^{2+} ~0.72–0.81) to the orthopyroxenite inner zones B to D (Fe^{3+}/Fe^{2+} ~0.33–0.44). The ranges of spinel compositions for the two samples, expressed as $Fe^{\#}$ ($Fe^{\#} = Fe^{2+}/(Fe^{2+}+Mg)$) and $Fe^{3+\#}$ ($Fe^{3+\#} = Fe^{3+}/(Fe^{3+}+Cr+Al)$) (Fig. 4a) are similar to the field of the other ultramafic xenoliths from the Beaunit layered complex (BLC in Fig. 4a) and also to the fields of many layered intrusions (compilations of Barnes and Roeder, 2001). Spinels from Beaunit fall into two compositional domains: (1) Al–Cr rich spinels in ultramafic xenoliths and (2) Fe-rich (Fe^{2+} and/or Fe^{3+}) spinels in mafic xenoliths (Fig. 4a).

The main accessory oxide phases of PBN 00-01 are Mg-ilmenite (Table 6) in the orthopyroxenite layer and rutile in central zones D and E. The Mg-ilmenite has quite variable compositions unrelated to its position in the sample. Its $Ti^{\#}$ ($Ti^{\#} = Ti/(Ti+Al+Cr)$) is nearly constant (0.97–0.99) whereas $Mg^{\#}$ varies from ~0.29 in zone B to ~0.45 in zone F. Mg-ilmenite also occurs in the orthopyroxenite and in the norite layers of PBN 00-03. The Ti number is nearly constant or slightly increases from zone B (0.97) to E (0.99) whereas the $Mg^{\#}$ decreases from 0.39 to 0.29. A rare small (1 μm in size) armacolite crystal (Table 6) occurs in the norite zone C of PBN 00-03.

Phlogopites ($Ph_{75–79}Ann_{20–25}Sdp_{0–4}$) occur in the central fine- and medium-grained orthopyroxenite zones C and D from PBN 00-01. They are titaniferous

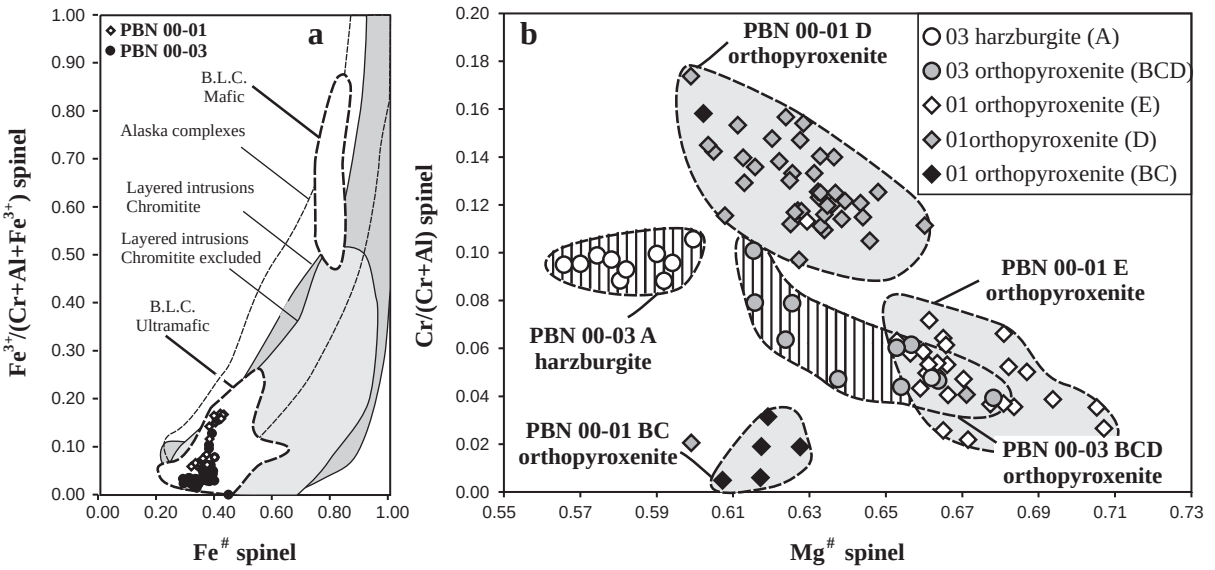

Fig. 4. (a) Spinel compositions of samples PBN 00-01 and PBN 00-03 compared to other terrestrial chromites (compilations of Barnes and Roeder, 2001), (b) Variation of spinel chemistry with lithological variations in the two studied samples. BLC=Beaunit Layered Complex.

with Ti ranging from 0.65 to 1.21 (a.p.f.u.). There is no relation between phlogopite composition and position in the sample. Numerous micrometre-scale crystals of pyrrhotite and pentlandite have been observed all along the profile in the sample PBN 00-01, whereas only a single grain has been found in zone C from PBN 00-03. Apatite is locally present in the orthopyroxenite layer of PBN 00-01. In this sample, minute zircon and srilankite $(Zr,Ti)O_2$ and a single 1.5 mm long zircon (that has been dated at 257 Ma by SIMS U–Th–Pb method; Féménias et al., 2003) have been found at the contact between zones B (orthopyroxenite) and A (norite). The presence of HFSE- and LILE-accessory phases: zircon, baddeleyite, zirconolite, loveringite, davidite occurred also in the Merensky reef (Ohnenstetter et al., 1998b) and could derive from extreme fractionation of a melt after compaction of the earlier cumulates (Ohnenstetter et al., 1998a).

5. Trace element compositional trends of major phases along the profile

Trace element concentrations of the major mineral phases (orthopyroxene, plagioclase and olivine) have been measured by in situ LA-ICP-MS analyses along a complete profile in the two samples. The analyses have been calibrated using the microprobe data presented before. Data are given in Tables 7 and 8. Each value represents an average of 4 to 7 spots obtained on the same grain. Representative REE patterns for the different minerals in each zone of the layered samples are shown in Figs. 5 and 6.

5.1. Sample PBN 00-01

Investigations have focused on orthopyroxene that is present in each zone defined in Fig. 2a, except for the thin norite zone A. Plagioclase of the norite (zone G) has also been analysed. Chondrite-normalised REE patterns (normalising values from McDonough and Sun, 1995) are presented for orthopyroxene and plagioclase on Fig. 5. Three types of orthopyroxene profile can be distinguished on the basis of the general shape of the REE patterns. (1) Orthopyroxene 1 is the most common type, occurring in zones B, C, E, F and G. It is characterised by low REE contents ($\sum$REE: 1.72 to 4.67 ppm), LREE depletion with $(La/Yb)_N$ in the range 0.004 to 0.19 and $(Gd/Yb)_N$ from 0.22 to 0.60 and a strong negative Eu anomaly ($(Eu/Eu^*)_N$=0.19 to 0.45). (2) Orthopyroxene 2 has been found in the central fine-grained orthopyroxenite zone D and is subsidiary in zones E and G. It is represented only by 1 or 2 grains in each zone (Fig. 5); it shows a smooth, LREE-depleted profile ($\sum$REE: 2.73 to 4.06 ppm; $(La/Yb)_N$: 0.009 to 0.028, $(Gd/Yb)_N$: 0.25 to 0.42), with only a slight Eu anomaly ($(Eu/Eu^*)_N$=0.85 to 0.98). (3) Orthopyroxene 3 is common in the central zone D (Fig. 5) and is characterised by variable LREE-enrichment ($(La/Yb)_N$=0.01–0.10 and $(Gd/Yb)_N$=0.30–0.72) superimposed on an LREE-depleted profile with no Eu anomaly $(Eu/Eu^*)_N \sim 1$. The three types of grains are not distinguishable petrographically. Plagioclase in norite zone G displays high REE content ($\sum$REE=75.6 ppm) with typical LREE enrichment ($(La/Yb)_N$=40.8 and $(Gd/Yb)_N$=6.9) and a strong positive Eu anomaly, $(Eu/Eu^*)_N$=3.9 (Fig. 5).

To summarise, the orthopyroxenes of PBN 00-01 show significant differences in REE contents and patterns within the large orthopyroxenite layer (zones B to F in Fig. 3). The common type 1 is LREE-depleted with strong negative Eu anomalies. Type 2 is also LREE-depleted but with no Eu anomaly and type 3, found only in the central fine-grained sub-layer, displays variable LREE enrichment superimposed on a general LREE-depleted pattern, with no Eu anomaly. Orthopyroxene of type 1 occurs on both sides (zones B, C, E, F, G) of the central zone D where type 3 orthopyroxene is observed. Type 2 has been observed only on one side (zones D to F) of the orthopyroxenite layer and in the neighbouring norite (zone G). HREE contents of orthopyroxene decrease regularly from zone B (Yb_N=7.5) to zone G (Yb_N=1.9), whereas the LREE content does not vary significantly except in norite zone G.

Some trace elements in orthopyroxene display nearly symmetrical trends across the whole sample (Fig. 6) while others display asymmetrical trends. The transition elements Cr, Ni and Co are significantly enriched in orthopyroxene from the fine- and medium-grained orthopyroxenite central area (Fig.

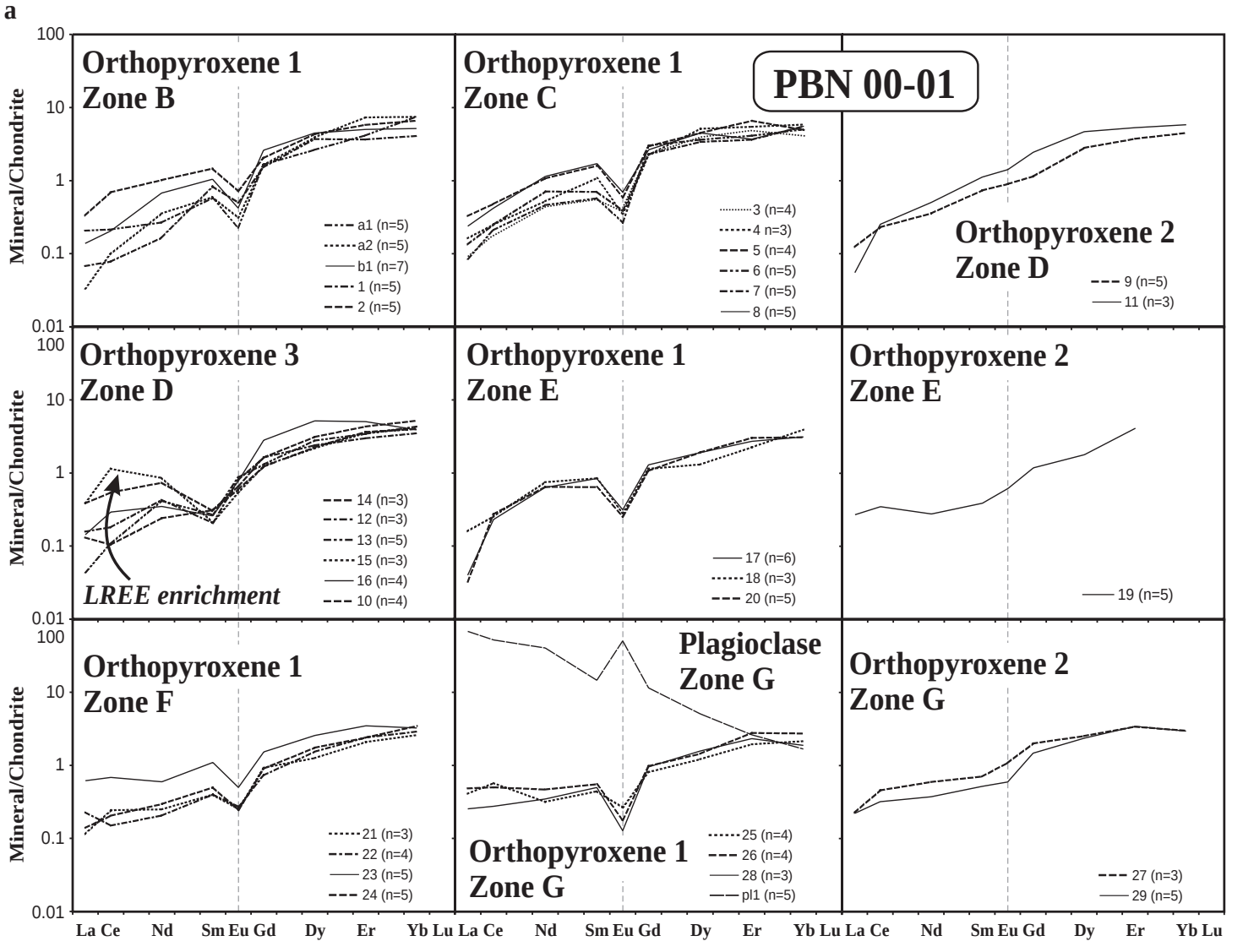

Fig. 5. REE patterns of orthopyroxenes and plagioclases in the different layers of PBN 00-01 and PBN 00-03. Concentrations of REE have been obtained by laser ablation ICP-MS. Normalising values are from McDonough and Sun (1995).

b

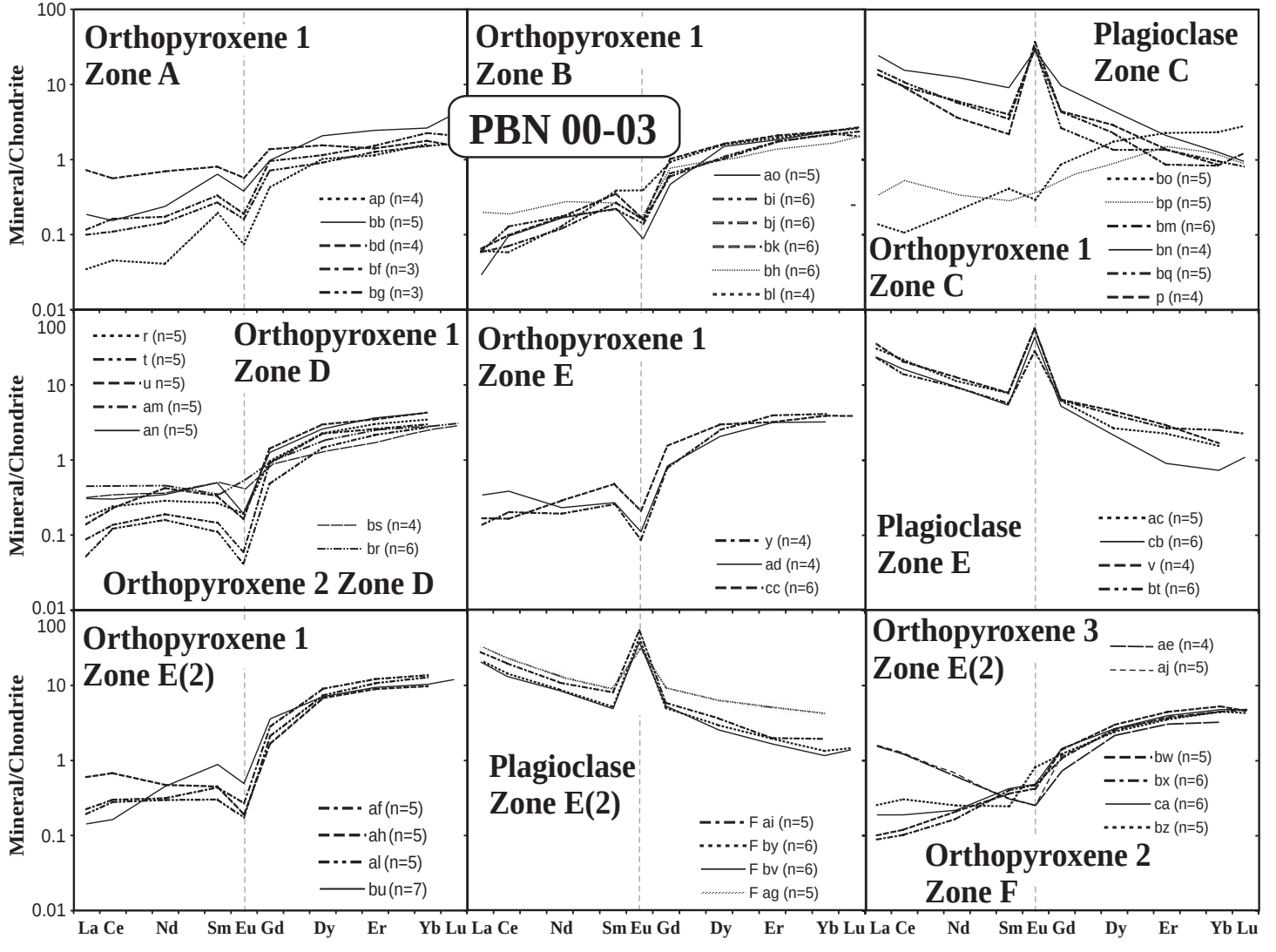

Fig. 5 (*continued*).

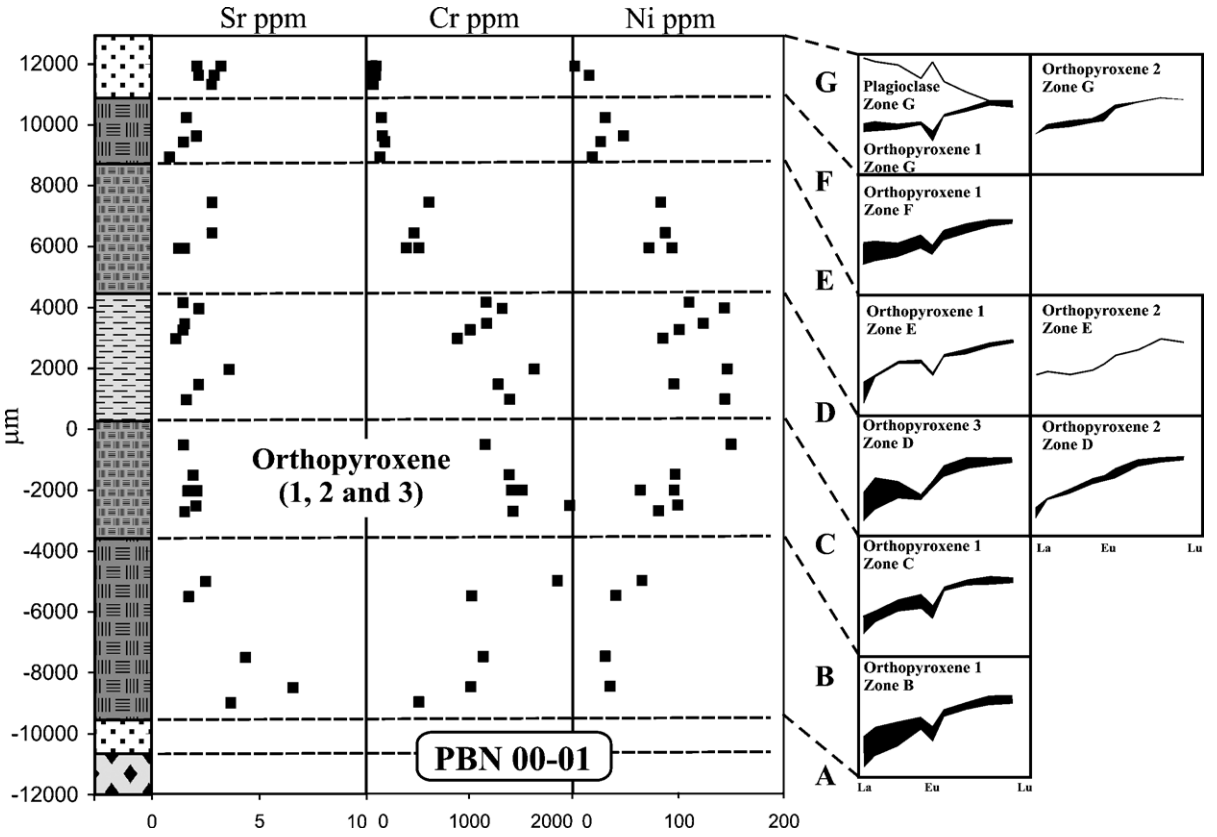

Fig. 6. Sr, Cr and Ni concentration variations in orthopyroxene from PBN 00-01 (measured by LA-ICP-MS) along the lithological profile.

6) with up to 1400 ppm Cr (one grain has 2000 ppm) and 140 ppm Ni. Their concentrations decrease on both sides to <500 ppm Cr and <20 ppm Ni. The Cr decrease is in fact asymmetrical, orthopyroxenes in zones B and C have higher Cr content (400–1000 ppm) than in zones E to G (300 to <100 ppm). The orthopyroxene with low Cr content coexists with Cr-rich spinel, while spinel is absent in the zone with Cr-rich orthopyroxene. The Zr content of numerous orthopyroxene grains is near or below detection limits (20 ppb), except for those located near the boundary between the orthopyroxenite and norite layers, where Zr is strongly enriched (5 to 700 ppm). This enrichment could be correlated to the local occurrence of rare zircon and srilankite. The Sr content of orthopyroxene is usually low (<3 ppm) but slightly higher (to 8 ppm) in the coarse-grained orthopyroxenite zone B, close to norite zone A (Fig. 6).

5.2. Sample PBN 00-03

Chondrite-normalised REE patterns of orthopyroxene and plagioclase from each zone (see Fig. 2b) are given in Fig. 5. Several types of orthopyroxene patterns can be distinguished that differ from zone to zone. In the harzburgite zone A, the profiles of four analysed orthopyroxenes are similar to that of type 1 orthopyroxene in PBN 00-01. They have rather low REE contents ($\sum$REE=0.87–2 ppm), LREE depletion ($(La/Yb)_N$=0.02–0.07 and $(Gd/Yb)_N$=0.26–0.47) and a strong negative Eu anomaly with $(Eu/Eu^*)_N$=0.27–0.54 (possibly enhanced by the poor precision on the Eu measurement at such low levels). An orthopyroxene close to the orthopyroxenite layer B is significantly enriched in LREE ($\sum$REE=2.24; $(La/Yb)_N$=0.40 and $(Gd/Yb)_N$=0.77). Most orthopyroxenes in the central orthopyroxenite layer (zones B, C and D) are also of type 1; they have overlapping REE contents with well defined negative Eu anoma-

lies ($(Eu/Eu^*)_N$=0.17–0.65) but ∑REE tends to be lower in zone B (1.26–1.64 ppm) than in zones C and D (1.34–2.70 ppm). Some grains of the orthopyroxenite layer and those of the thin central norite zone C have only a slight Eu anomaly ($(Eu/Eu^*)_N$=0.5–0.98), similar to type 2 of PBN 00-01. In the norite layer (zone E), the orthopyroxenes display either type 1 distribution patterns with slightly higher REE content (∑REE=2.14–3.74 ppm) but similar LREE depletion ($(La/Yb)_N$=0.03–0.16 and $(Gd/Yb)_N$=0.23–0.49) or patterns similar to type 3. Some orthopyroxenes of the outer part of norite zone E resemble to type 2 in their LREE depletion ($(La/Yb)_N$=0.02–0.06) but the Eu anomaly is poorly marked. Orthopyroxene 3 is characterised by a strong LREE enrichment ($(La/Yb)_N$=0.35–0.47 with $(Gd/Yb)_N$=0.22–0.25) with a well defined Eu anomaly ($(Eu/Eu^*)_N$=0.42–0.53), this enrichment seems to overprint a normal (=type 1) pattern. Orthopyroxenes of type 3 occur in the central part of the norite layer as very small grains (<200 μm) that are close to the laser spot size, limiting the grains available for analyses.

The overall variations of REE contents of the various types of orthopyroxene along the profile are essentially controlled by HREE contents, that show a slight but continuous increase from zone A to zone E (Fig. 5), except for orthopyroxene type 3 that has a strong LREE enrichment. Plagioclase in the thin norite zone C is significantly enriched in REE (∑REE=14.4–15.9 ppm) compared to coexisting orthopyroxene; it has a strong LREE enrichment ($(La/Yb)_N$=15.7–16.2 and $(Gd/Yb)_N$=2.8–5.2) and strong positive Eu anomalies ($(Eu/Eu^*)_N$: 3.0–6.9). One grain has significantly higher REE content (∑REE=26.7 ppm) and a lower Eu anomaly ($(Eu/Eu^*)_N$=11.6). Plagioclases of the norite zone E have similar patterns, with higher REE contents (∑REE=23.1–38.8 ppm).

6. Discussion: metamorphic versus magmatic origin

6.1. Asymmetrical to symmetrical evolution trends

In layered rocks, variations of mineralogical and chemical compositions as well as textures define several types of pattern that could reflect a complex magmatic history (fractional crystallisation, mineral sorting…) and/or late- to post-magmatic processes. At the scale of a layered intrusion, these variations are classically interpreted in terms of periodic pulses of magma and/or the static evolution of a magma body in the chamber (e.g. McBirney and Nicolas, 1997 for the Skaergaard intrusion). These variations can be described as continuous or discontinuous, asymmetrical or symmetrical features (Fig. 7).

In periodic magma replenishment or in a closed system, continuous asymmetrical profiles (Fig. 7d–f) could be due to crystallisation fronts, chemical fronts or interactions between a newly injected layer (sill, new pulse of magma…) and the enclosing partially or totally crystallised earlier layers. These profiles may be related to chemical changes in the magma (differentiation and/or new injection) or Soret fractionation (Latypov, 2003a) and/or to overall or axial changes in thermobarometric conditions (height in the magma chamber or distance from wall-rock for example). Symmetrical profiles (Fig. 7a–c) involve either injection as a dyke or sill (Latypov, 2003b) or plumbed percolation (channelling) by a fluid and/or a liquid. Profiles can be limited to a single layer (no interaction with surrounding wall-rocks, Fig. 7b) or can affect the neighbouring layers by passive or active interactions with the wall-rocks (Fig. 7a, c and d). In the case of active interactions with the wall-rock, chemical changes by contamination/assimilation (leading to enrichment and/or depletion) and thermodynamic effects (cooling) are expected. The wall-rock itself can be modified mineralogically, chemically and/or texturally. Each of the theoretical features described above should be discussed in relation to a geological process, according to the type of profile observed (Latypov, 2003a,b).

In the Beaunit layered xenoliths, the complex patterns observed in the distribution of major and trace elements, as well as in the distribution of accessory phases and textures, cannot be ascribed to a single mechanism related to the mode of emplacement and differentiation. Nevertheless, each feature has probably recorded some part of an overall process and could be discussed with respect to its relative importance for the formation of the igneous layering and to its chronological position in the sequence of events.

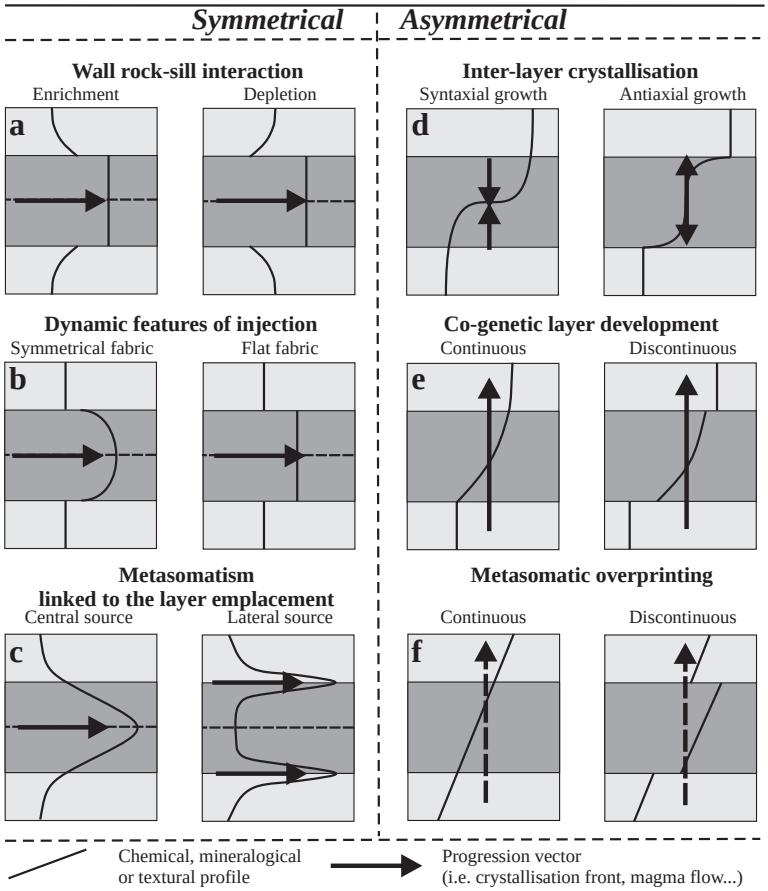

Fig. 7. Sketch model to illustrate the various physical or chemical processes that can affect the distribution profiles of elements, minerals and/or textures in an hypothetical layered sample consisting of 3 layers.

6.2. Dynamic solid-state features

Both layered samples have a central orthopyroxenite layer. The profiles of these layers are roughly symmetrical with respect to texture and modal compositions (Fig. 2); the variation of orthopyroxene composition of PBN 00-01 is also symmetrical (Fig. 3a). These symmetrical profiles cannot be explained by a reaction mechanism between the orthopyroxenites and the neighbouring lithologies because for PBN 00-01, the orthopyroxenite layer is sandwiched between two norite layers while, for PBN 00-03, the orthopyroxenite is bounded by a harzburgite and a norite layer. The shape preferred orientation of the harzburgite layer of PBN 00-03 suggests that crystallisation and textural development of this layer took place before consolidation of the orthopyroxenite layer. Furthermore, grain size variations in the orthopyroxenite layer in PBN 00-01 argue for an intrinsic textural acquisition process, independent of the enclosing norite in which polygonal sub-solidus recrystallisation and grain size homogenisation took place earlier. So we suggest that the shape preferred orientation on one hand and the crystal size distribution on the other hand have to be considered as solid-state deformation features, that occurred at the deep crustal level of emplacement of the Beaunit complex. This grain size variation could be explained by a dynamic recrystallisation process, possibly reflecting a late-shearing mechanism; in that hypothesis, the central fine-grained zone would represent the zone of maximum stress. As this deformation process affected completely solidified rocks, it obviously occurred after the crystallisation

of the layers. Nevertheless, the inter-stratified position of the orthopyroxenite layer could be related to band-on-band movement associated with gravitative displacement and/or magma convection (McBirney and Nicolas, 1997). Moreover, the location of accessory phases in PBN 00-03 orthopyroxenite layer argues for a syn-axial crystallisation from a residual interstitial liquid enriched in incompatible elements, away from the layer boundaries squeezed into the pre-existing layered section. In the Bushveld complex, the pyroxenites of the Merensky Reef also contain numerous accessory minerals (zircon, baddeleyite, zirconolite, loveringite, davidite…; Ohnenstetter et al., 1998a) and are strongly enriched in HFS- and LIL-elements compared to the adjacent norites. They have been related to the extreme fractionation of a melt after compaction of earlier cumulates (Ohnenstetter et al., 1998b). Moreover, trace element modelling (Arndt et al., in press) suggests that the Mg-rich magma that gave rise to the Merensky Reef pyroxenites is strongly enriched in incompatible elements; this liquid has probably been contaminated before entering the main Bushveld magma chamber.

The structural features observed in the Beaunit layered xenoliths can tentatively be explained by the injection of a thin liquid layer of orthopyroxene-rich composition along the pre-existing boundary between two previously consolidated layers. This micro-injection has sill-like characteristics.

6.3. Chemical features

Mineralogical as well as chemical profiles have been described for the two layered samples. Chemical trends (Figs. 3–6) usually show strong variations at the centimetre scale. For example, the $Mg^{\#}$ of orthopyroxene in PBN 00-03 varies from 72 to 81 over 1 cm of stratigraphic height (Fig. 3e). These variations are similar to those described in typical stratiform intrusions (i.e. Lower and Critical Zones of the Bushveld complex (Eales and Cawthorn, 1996); banded series of the Stillwater intrusion (McCallum, 1996)) but there is a huge difference of scale: in the layered intrusions, a variation of 10 in the $Mg^{\#}$ of orthopyroxene occurs over several tens or hundred of metres of cumulate rocks. Therefore, different processes have to be invoked to explain the distribution of elements and the compositional trends of each phase in the Beaunit layered samples. Each profile can result either from a single mechanism (i.e. reaction between the orthopyroxenite liquid and pre-existing lithologies) or from several mechanisms occurring along the same lithological boundary. The multi-stage emplacement process, deduced from the dynamic solid-state features, would suggest the overprinting of a primary chemical signature.

The observed chemical concentration trends can be possibly related to several processes:

a) a crystallisation trend associated with a residual liquid enriched in incompatible elements and relatively depleted in compatible elements. The LREE enrichment observed for some orthopyroxenes (type 3 on Fig. 5) could be related to this kind of mechanism. The complete profiles could result from syn-axial versus anti-axial crystallisation and/or mechanical segregation due to flow differentiation (Bagnold, 1954; Komar, 1972a,b, 1976). Indeed, the thin central norite layer from the PBN 00-03 orthopyroxenite zone contains clinopyroxene, phlogopite, oxides and apatite, that are commonly associated with a more evolved residual liquid, suggesting syn-axial crystallisation. In contrast, orthopyroxenes from PBN 00-01 orthopyroxenite layer show symmetrical primary patterns for $Mg^{\#}$ (Fig. 3) and Cr and Ni contents (Fig. 6), suggesting the accumulation of orthopyroxene crystals in the central zone perhaps by flow differentiation or anti-axial crystallisation;
b) diffusion profiles are observed, for example, at the contact between two lithologies with contrasting chemistry (e.g. $Mg^{\#}$ of spinel between harzburgite layer A and orthopyroxenite layer B of PBN 00-03; Fig. 3h), suggesting local open-system conditions;
c) local assimilation of wall-rock by a liquid injected along the boundary between pre-existing layers. This process could dilute or enrich the liquid in some elements, recycle and/or partially melt the pre-existing phases. In PBN 00-01, there is a local enrichment of Sr in orthopyroxenes of the coarse-grained orthopyroxenite at the contact with the plagioclase-rich norite (Fig. 6). The local Zr enrichment on both sides of the orthopyroxenite

layer in PBN 00-01 may be due to remobilisation of evolved liquid along boundaries;

d) percolation of a newly injected magma along cracks of an already consolidated wall-rock. The layer of Mg-rich magma (picrobasalt or boninite) crystallised as orthopyroxenite layer. Similar orthopyroxenite veinlets or dykes have been observed in ophiolite complexes and Alaskan-type complexes (Paktunc and Cabri, 1995), and in ultramafic intrusives (Pal and Mitra, 2004). This magma could lead to local enrichment of the layered wall-rocks before their late sub-solidus recrystallisation that blurs the layering;

e) metasomatic enrichment by a fluid derived either from the lately injected magma layer or from an external source (Fig. 7c). This event could induce chemical and/or mineralogical changes along layer boundaries or in the centre of a layer (Naslund and McBirney, 1996). In PBN 00-01, the presence of Ti-phlogopite, apatite and augite in the central part of the orthopyroxenite layer records a local hydrous environment. LREE enrichment observed in type 3 orthopyroxenes (Fig. 5) of the central orthopyroxenite zone could also be due to such metasomatism.

Chemical signatures for a given mineral phase are also quite variable within a single zone of a layered sample. For example, orthopyroxenes in PBN 00-03 (Fig. 5) display variations in LREE enrichment and Eu anomalies. Several mechanisms can in theory explain these variations:

a) the mechanisms described above at the scale of a layer could operate at the mineral-scale, within a layer;

b) a heterogeneous overprinting of one of the mechanisms described above;

c) the primary cumulus or intercumulus signature of a phase could have been partially preserved. These signatures would reflect the partition coefficients (at given P–T conditions) for these phases equilibrated with an evolving liquid during crystallisation;

d) sub-solidus reequilibration of orthopyroxene could induce changes in trace element patterns, depending on the nature of the neighbouring phases and/or of the amount and nature of the lost intercumulus materials (e.g. Barnes, 1986);

6.4. Static solid-state processes

Solid-state processes such as sub-solidus recrystallisation may have occurred during cooling of the Beaunit layered complex at deep crustal levels (as shown by Zingg (1996) for the layered rocks of the Bushveld complex). P–T granulite facies conditions prevailing during emplacement were estimated at T ~800 °C and P ~0.7–1 GPa (Faure et al., 2001; Féménias et al., 2001). Sub-solidus polygonal textures are not present in all Beaunit samples. Magmatic websterites indeed frequently display primary features like twinning and exsolution lamellae of clinopyroxene in orthopyroxene. In contrast, plagioclase and orthopyroxene in unlayered norite xenoliths (unpublished data) are usually unzoned. Cores and rims of orthopyroxenes analysed in the present study (Fig. 5) have, within analytical error, the same major element compositions and the same REE concentrations. Moreover, sub-solidus recrystallisation already started soon after the onset of crystallisation and not only after acquisition of the final layering. Indeed, the shape fabric of the harzburgite layer (PBN 00-03) reflects an early sub-solidus stage (stage 1) whereas the equant grain size texture observed at the boundaries between the central orthopyroxenite and the external layers may be interpreted as a secondary sub-solidus stage. Following the same way of reasoning, we can argue that polygonal texture acquisition in PBN 00-01 can also be related to this stage “2”. Thus, the crystal size variation observed in the central orthopyroxenite layer has to be interpreted as a late sub-solidus stage “3”. Each sub-solidus recrystallisation stage presumably enhanced elemental diffusion. As a result, chemical profiles and signatures within a single grain as well as between adjacent grains have probably been smeared out to a large degree.

6.5. An alternative hypothesis: the Soret fractionation

For sample PBN 00-03, Latypov (pers. communic.) suggests an alternative hypothesis on the basis of the compositional variations of the main

minerals, orthopyroxene and plagioclase (Fig. 3). Indeed, the En content of orthopyroxene increases from norite zone E (En 72–76) to the orthopyroxenite (En 76 in zone D and En 78–80 in zone B) and to the harzburgite (En 80 in zone A). The An content of the plagioclase increases from An 60 (zone E) to An 90 (zone C). There is no plagioclase in the harzburgite. In fact, it is possible that the sampled xenolith would represent only a part of a bigger specimen that has a central harzburgite layer successively mantled by orthopyroxenite and norite layers. The succession of fractionated phases, ol+opx+liq (harzburgite), opx+liq (orthopyroxenite), opx+pl+liq (norite) is indeed consistent with a normal fractionation trend. According to this hypothesis, all the layers of PBN 00-03 would belong to the same sill-like intrusion for which the host rocks have not been preserved in the sampled xenolith. The layered sample would display a D-shaped compositional profile with a central primitive harzburgite zone and more evolved (orthopyroxenite and norite) margins. The phase and cryptic layering could be attributed to a single Soret fractionation process (Latypov, 2003a,b).

We do not agree with this model for several reasons: (1) the harzburgite zone displays a well-marked shape orientation that is completely absent in the neighbouring orthopyroxenite–norite layers; (2) the succession of layers (norite–orthopyroxenite–harzburgite) has rarely been observed in the numerous layered xenoliths of Beaunit that we have examined; so this succession is an exception rather than the general rule; (3) the $Mg^{\#}$ of spinel is significantly higher in the orthopyroxenite zone (0.61–0.68) than in the harzburgite zone (0.56–0.60) (Fig. 4); (4) the distribution of accessory phases in the orthopyroxenite zone favours a syn-axial crystallisation from a liquid enriched in incompatible elements.

7. Conclusions

Our study points out that layering, especially micro-layering, cannot be used systematically as a stratigraphic temporal indicator of magmatic differentiation. Sill-like intrusions may occur at all scales (few mm up to several metres) during crystallisation in a magma chamber and therefore during the build-up of the magmatic layering and concomitant chemical evolution. In the Merensky reef orthopyroxenites, trace elements are also strongly enriched compared to adjacent norites and modelling reveals major differences of the two types of rocks. The Merensky pyroxenites are formed from a liquid with far higher concentrations of incompatible trace elements than the liquid producing the norites (Arndt et al., in press).

The layered xenoliths from Beaunit show evidence of a complex multi-stage history, some of the early stages could have been partially or totally overprinted by the later stages. We summarise our understanding of the history of the two studied layered nodules by the following sequence of five events.

7.1. PBN 00-01

1) Formation of norites, by fractional crystallisation and accumulation of both plagioclase (with positive Eu anomaly) and orthopyroxene (with negative Eu anomaly) that could represent a cotectic assemblage;
2) A first episode of sub-solidus recrystallisation under granulite facies conditions leading to the formation of polygonal texture and the chemical homogenisation of the major mineral phases;
3) Injection of an orthopyroxene-rich liquid as a thin sill. This injection leads to concomitant metasomatic reaction with the surrounding norite cumulates. The partial remobilisation of some elements (e.g. Zr, Sr) in relation with the channelling of the liquid along layer boundaries could cause a local Zr enrichment that locally leads to the crystallisation of zircon and srilankite, as observed under granulite facies conditions by Bingen et al. (2001);
4) The symmetrical crystal size distribution observed in the orthopyroxenite layer could tentatively be related to a non-coaxial solid-state deformation event or to a late-cooling shearing mechanism. The central fine-grained orthopyroxenite zone probably represents the zone of maximum stress;
5) During or after the previous stage, hydrous and fluid-enriched mineral phases (phlogopite, apatite...) develop in the fine-grained central zone D. They crystallise from a fluid-rich phase that could be the source of the LREE-enrichment observed in some orthopyroxenes of this central zone.

7.2. PBN 00-03

1) Fractional crystallisation and accumulation of olivine and orthopyroxene to form the harzburgite layer. The orthopyroxenites represent later cumulates, formed from a residual liquid after plagioclase fractionation. It has been shown experimentally (Müntener et al., 2001) that a low H_2O content (<3%) in the liquid stabilises plagioclase earlier than amphibole. This could also explain the low proportion of hydrous phases in all the Beaunit cumulates;
2) Dynamic recrystallisation of olivine and orthopyroxene in the harzburgite has induced a shape fabric and polygonal texture. This was presumably a late- to post-cumulate process;
3) Plagioclase and orthopyroxene accumulate to form the norite layer. The orthopyroxenes with negative Eu anomaly have accumulated together with plagioclase with positive Eu anomaly and therefore probably reflect a cotectic fractionation assemblage;
4) Injection of a thin liquid layer of orthopyroxenite composition along the harzburgite–norite boundary as a micro-sill. This liquid and the associated fluid have partially overprinted the previous magmatic assemblages and induced a local metasomatism. This injected liquid could have been enriched by assimilation and/or recycling of the first crystallised phases;
5) Development of a final polygonal texture and homogenisation of the primary chemical profiles have presumably taken place during a second, partial, sub-solidus recrystallisation process.

Some broad generalisations on the origin of layering in deep layered complexes can be proposed. Xenoliths that are commonly called meta-igneous (i.e. Dostal et al., 1980 and Downes et al., 1990 for the French Massif Central crustal xenoliths) by reference to their polygonal texture, are in fact dominantly of igneous origin. Their textures have been developed during sub-solidus recrystallisation contemporaneous with the emplacement, as has been shown in this study for the two layered samples. Indeed, the deep crustal environment (granulite facies conditions) of the Beaunit layered complex contributed to a strong increase of the intensity of the sub-solidus processes, essentially by static recrystallisation occurring during emplacement. Nevertheless, magma movements, mainly at the floor of the chamber, may induce local, non-coaxial, dynamic deformation by lamination processes.

This study has shown that the magmatic xenoliths of Beaunit have not been overprinted by a post-emplacement HT-MP metamorphism, but crystallised and recrystallised directly under granulite facies conditions during the Permian. Consequently, the granulitisation of the deep crust in the French Massif Central that has been considered by some authors (Costa and Rey, 1995) to be of orogenic origin, is more probably contemporaneous with the late- to post-orogenic (Vielzeuf and Pin, 1991) magmatic underplating event (Féménias et al., 2003) that corresponds to the emplacement of hot mafic magma, preceding the opening of the Liguro–Piemont oceanic basin.

Acknowledgements

DD wants to dedicate this work to Jean-Clair Duchesne with whom he has collaborated fruitfully and (more importantly) in a friendly way during the last 25 years.

The constructive and thorough reviews of H. Downes, M. Grégoire and R. Latypov and the editorial comments of J. Vander Auwera (Guest Editor) are greatly acknowledged. We thank S. Barda and F. Diot (University of Nancy I) for technical help at the CAMECA SX50 Microprobe.

References

Arndt, N., Jenner, G., Ohnenstetter, M., Deloule, E., Wilson, A., in press. Trace element in the Merensky Reef and adjacent norites, Busveld Complex. South Africa. Miner. Depos.

Bagnold R.A., 1954. Experiments on a gravity-free dispersion of large solid spheres in a Newtonian fluid under shear. Proc. R. Soc. Lond. 225, 49–63.

Barnes S.J., 1986. The effect of trapped liquid crystallisation on cumulus mineral compositions in layered intrusions. Contrib. Mineral. Petrol. 93, 524–531.

Barnes S.J., Roeder P.L., 2001. The range of spinel compositions in terrestrial mafic and ultramafic rocks. J. Petrol. 42, 2279–2302.

Baudry D., Camus G., 1970. Les maars de la chaîne des Puys (formations volcaniques du Massif central français). Bull. Soc. Géol. Fr. XII (2), 185–189.

Berger, E., 1981. Enclaves ultramafiques, mégacristaux et leur basaltes-hôtes en contexte océanique (Pacifique sud) et continental (Massif Central français). Thèse Doct. Etat, Univ. Orsay, 467 pp.

Bingen B., Austrheim H., Whitehouse M., 2001. Ilmenite as a source for zirconium during high-grade metamorphism? Textural evidence from the caledonides of Western Norway and implications for zircon geochronology. J. Petrol. 42, 355–375.

Brousse R., Rudel A., 1964. Bombes de péridotites, de norites, de charnockites et de granulites dans les scories du puy Beaunit. C. R. Acad. Sci. Paris 259, 185–188.

Camus, G., 1975. La Chaîne des Puys. Etude structurale et volcanologique. Thèse Doct. Etat, Univ. Clermont-Ferrand II, 321 pp.

Cawthorn, R.G. (Ed.), 1996. Layered Intrusions. Elsevier Science B.V. 531 pp.

Costa S., Rey P., 1995. Lower crustal rejuvenation and growth during post-thickening collapse: insights from a crustal cross section through a Variscan metamorphic core complex. Geology 23, 905–908.

Dostal J., Dupuy C., Leyreloup A.F., 1980. Geochemistry and petrology of meta-igneous granulitic xenoliths in Neogene volcanic rocks of the Massif Central, France – implication for the lower crust. Earth Planet. Sci. Lett. 50, 31–40.

Downes H., Dupuy C., 1987. Textural, isotopic and REE variations in spinel peridotites xenoliths, Massif Central, France. Earth Planet. Sci. Lett. 82, 121–135.

Downes H., Dupuy C., Leyreloup A.F., 1990. Crustal evolution of the Hercynian belt of Western Europe: evidence from lower-crustal granulitic xenoliths (French Massif Central). Chem. Geol. 83, 209–231.

Downes H., Reichow M.K., Mason P.R.D., Beard A.D., Thirlwall M.F., 2003. Mantle domains in the lithosphere beneath the French Massif Central: trace elements and isotopic evidence from mantle clinpyroxenes. Chem. Geol. 200, 71–87.

Eales H.V., Cawthorn R.G., 1996. The Bushveld complex. In: Cawthorn, R.G. (Ed.), Layered Intrusions. Elsevier Science B.V, pp. 181–229.

Faure F., Trolliard G., Montel J.-M., Nicollet C., 2001. Nano-petrographic investigation of a mafic xenolith (maar de Beaunit, Massif Central, France). Eur. J. Mineral. 13, 27–40.

Féménias O., Mercier J.-C.C., Demaiffe D., 2001. Petrology of ultramafic xenoliths from the Puy Beaunit (French Massif Central): an unusual occurrence for the sub-continental mantle. C. R. Acad. Sci. Paris IIA (332), 535–542.

Féménias O., Coussaert N., Bingen B., Whitehouse M., Mercier J.-C.C., Demaiffe D., 2003. A Permian underplating event in late- to post-orogenic tectonic setting. Evidence from the mafic-ultramafic layered xenoliths from Beaunit (French Massif Central). Chem. Geol. 199, 293–315.

Hunter R.H., 1996. Texture development in cumulate rocks. In: Cawthorn, R.G. (Ed.), Layered Intrusions. Elsevier Science B.V. pp. 77–101.

Irvine T.N., 1982. Terminology for layered intrusions. J. Petrol. 23, 127–162.

Komar P.D., 1972a. Mechanical interactions of phenocrysts and flow differenciation of igneous dikes and sills. Geol. Soc. Am. Bull. 83, 973–988.

Komar P.D., 1972b. Flow differentiation in igneous dikes and sills; profiles of velocity and phenocryst concentration. Geol. Soc. Am. Bull. 83, 3443–3447.

Komar P.D., 1976. Phenocryst interactions and the velocity profile of magma flowing through dikes or sills. Geol. Soc. Am. Bull. 87, 1336–1342.

Latypov R.M., 2003a. The origin of marginal compositional reversals in basic–ultrabasic sills and layered intrusions by Soret fractionation. J. Petrol. 44, 1579–1618.

Latypov R.M., 2003b. The origin of basic–ultrabasic sills with S-, D- and I-shaped compositional profiles by in situ crystallisation of a single input of phenocryst-poor parental magma. J. Petrol. 44, 1619–1656.

Le Maitre R.W., 2002. A Classification of Igneous Rocks and Glossary of Terms. Recommendations of the International Union of Geological Sciences Subcommission on the Systematics of Igneous Rocks. Blackwell Scientific Publications. 193 pp.

Lenoir X., Garrigo C.J., Bodinier J.-L., Dautria J.-M., 2000. Contrasting lithospheric mantle domains beneath the Massif Central (France) revealed by geochemistry of peridotites xenoliths. Earth Planet. Sci. Lett. 181, 359–375.

Leyreloup, A.F., 1973. Le socle profond en Velay d'après les enclaves remontées par les volcans néogènes, son thermométamorphisme et sa lithologie: granites et série charnockitique (Massif Central français). Thèse 3ème cycle, Univ. Nantes, 356 pp.

Maier W.D., Barnes S.-J., 1998. Concentrations of rare earth elements in silicate rocks of the lower, critical and main zones of the Bushveld Complex. Chem. Geol. 150, 85–103.

Mc Birney A.R., Hunter R.H., 1995. The cumulate paradigm reconsidered. J. Geol. 103, 114–122.

McBirney A.R., Nicolas A., 1997. The Skaergaard layered series: Part II. Magmatic flow and dynamic layering. J. Petrol. 38, 569–580.

McCallum I.S., 1996. The stillwater complex. In: Cawthorn, R.G. (Ed.), Layered Intrusions. Elsevier Science B.V., pp. 441–483.

McDonough W.F., Sun S.S., 1995. The composition of the Earth. Chem. Geol. 120, 223–253.

Mercier, J.-C.C., 1972. Structure des péridotites en enclaves dans quelques basaltes d'Europe et d'Hawaii. Regards sur la constitution du manteau supérieur, Thèse 3ème cycle, Univ. Nantes.

Müntener O., Kelemen P.B., Grove T.L., 2001. The role of H_2O during crystallization of primitive arc magmas under uppermost mantle conditions and genesis of igneous pyroxenites: an experimental study. Contrib. Mineral. Petrol. 141, 643–658.

Naslund H.R., McBirney A.R., 1996. Mechanisms of formation of igneous layering. In: Cawthorn, R.G. (Ed.), Layered Intrusions. Elsevier Science B.V., pp. 1–43.

Ohnenstetter M., Arndt N., Lee C.A., 1998a. Occurrence and compositional variation of HFSE- and LILE-bearing oxides in the Merensky Reef, Rustenburg area. 8th International Platinum Symposium, Johannesburg. South African Institute of Mining and Metallurgy, pp. 301–303.

Ohnenstetter M., Arndt N., Lee C.A., 1998b. The Merensky Reef evolution from the HFSE- and LILE bearing oxides and related silicates. 8th International Platinum Symposium, Johannesburg. South African Institute of Mining and Metallurgy, pp. 297–299.

Paktunc A.D., Cabri L.J., 1995. A proton- and electron-microprobe study of gallium, nickel and zinc distribution in chromian spinel. Lithos 35, 261–282.

Pal T., Mitra S., 2004. P-T-fo2 controls on a partly inverse chromite-bearing ultramafic intrusive: an evaluation from the Sukinda Massif, India. J. Asian Earth Sci. 22, 483–493.

Philpotts A.R., Dickson L.D., 2002. Millimeter-scale modal layering and the nature of the upper solidification zone in thick flood-basalt flows and other sheets of magma. J. Struct. Geol. 24, 1171–1177.

Pouchou J.L., Pichoir F., 1991. Quantitative analysis of homogeneous or stratified microvolumes applying the method "PAP". In: Heinrich, K.J.F., Newbury, D.E. (Eds.), Electron Probe Quantification. Plenum Press, New York, pp. 3–75.

Rosseel, J.B., 1996. Synthèse chrono-magmatologique de la Chaîne des Puys. Unpublished diploma (DEA). Univ. B. Pascal, Clermont-Ferrand II. 50 pp.

Streckeisen A.L., 1974. Classification and nomenclature of plutonic rocks. Geol. Rundsch. 63, 773–786.

Vielzeuf D., Pin C., 1991. Granulites orthodérivées d'âge tardi-hercynien; exemple de la norite de Treilles, Corbières (Aude, France). Bull. Soc. Géol. Fr. 6, 1057–1066.

Wager L.R., Brown G.M., 1968. Layered Igneous Rocks. Oliver and Boyd, Edinburgh. 588 pp.

Wager L.R., Deer W.A., 1939. Geological investigations in East Greenland: Part III. The petrology of the Skaergaard intrusion, Kangerdlugssuag, East Greenland. Medd. Gronl. 105, 1–352.

Wager L.R., Brown G.M., Wadsworth W.J., 1960. Types of igneous cumulates. J. Petrol. 1, 73–85.

Zingg J., 1996. Recrystallization and the origin of layering in the Bushveld Complex. Lithos 37, 15–37.